Polypyrimidine Tract Binding Proteins are essential for B cell development

Authors:

Elisa Monzón-Casanova[1,2*], Louise S. Matheson[1], Kristina Tabbada[3], Kathi Zarnack[4], Christopher W. J. Smith[2] and Martin Turner[1*]

Affiliations:

[1]Laboratory of Lymphocyte Signalling and Development, The Babraham Institute, Cambridge, UK;

[2]Department of Biochemistry, University of Cambridge, Cambridge, UK;

[3]Next Generation Sequencing Facility, The Babraham Institute, Cambridge, UK;

[4]Buchmann Institute for Molecular Life Sciences, Goethe University Frankfurt, Frankfurt am Main, Germany

*Corresponding authors:

Elisa Monzón-Casanova (elisa.monzon-casanova@babraham.ac.uk) and Martin Turner (martin.turner@babraham.ac.uk)

Abstract

Polypyrimidine Tract Binding Protein 1 (PTBP1) is a RNA-binding protein (RBP) expressed throughout B cell development. Deletion of *Ptbp1* in mouse pro-B cells results in upregulation of PTBP2 and normal B cell development. We show that PTBP2 compensates for PTBP1 in B cell ontogeny as deletion of both *Ptbp1* and *Ptbp2* results in a complete block at the pro-B cell stage and a lack of mature B cells. In pro-B cells PTBP1 ensures precise synchronisation of the activity of cyclin dependent kinases at distinct stages of the cell cycle, suppresses S-phase entry and promotes progression into mitosis. PTBP1 controls mRNA abundance and alternative splicing of important cell cycle regulators including CYCLIN-D2, c-MYC, p107 and CDC25B. Our results reveal a previously unrecognised mechanism mediated by a RBP that is essential for B cell ontogeny and integrates transcriptional and post-translational determinants of progression through the cell cycle.

Introduction

Antibody diversity is crucial to fight infections and is generated throughout B cell development by the orderly recombination of V(D)J gene segments of the immunoglobulin heavy (Igh) and light (Igl) chain loci. Igh-recombination at the pro-B cell stage typically occurs before Igl recombination in B cell ontogeny (**Figure S1A**). Pro-B cells can be separated into fractions (Fr) B and C according to Hardy's criteria (Hardy *et al*, 1991), with D to J gene segment recombination occurring in FrB pro-B cells prior to V to DJ recombination in FrC pro-B cells (Hardy & Hayakawa, 2003). Successful VDJ recombination of the Igh chain locus is coupled with a rapid proliferative expansion of early-pre-B cells (FrC') and the subsequent return to quiescence permissive for recombination at the Igl chain loci in late-pre-B cells (FrD) (Herzog *et al*, 2009). V(D)J recombination occurs during the G0/G1 phase of the cell cycle (Schlissel *et al*, 1993) and the RAG proteins, which are essential for V(D)J recombination, are degraded upon entry into S-phase, suppressing further recombination (Li *et al*, 1996). The alternation between proliferative and non-proliferative stages during B cell development is precisely controlled to maintain genomic integrity (Herzog *et al*, 2009; Clark *et al*, 2014). Several factors have been identified that suppress proliferation in late-pre-B cells and allow Igl recombination. These include B cell translocation gene 2 (BTG2) and protein arginine methyl transferase 1 (PRMT1) (Dolezal *et al*, 2017), the signal transducers RAS (Mandal *et al*, 2009) and dual specificity tyrosine-regulated kinase 1A (DYRK1A) (Thompson *et al*, 2015) and the transcription factors interferon regulatory factor-4 and -8 (IRF4, IRF8) (Lu *et al*, 2003), IKAROS and AIOLOS (Ma *et al*, 2010), BCL-6 (Nahar *et al*, 2011) and FOXO3a (Herzog *et al*, 2008). In pro-B cells, IL-7 promotes cell cycle progression (Clark *et al*, 2014) and the RNA-binding proteins (RBPs) ZFP36L1 and ZFP36L2 suppress

proliferation, allowing Igh chain recombination and B cell development (Galloway *et al*, 2016). Thus, by comparison to pre-B cells the mechanisms and genes that control proliferation in pro-B cells remain poorly understood.

Transcription factors act to determine which genes are transcribed and the tempo of transcription. A significant body of work has identified a network of transcription factors that control the development and identity of B cells (Busslinger, 2004). Amongst these, FOXO1 is essential for progression after the pro-B cell stage and to induce expression of *Rag* genes (Dengler *et al*, 2008; Amin & Schlissel, 2008). After transcription, numerous RBPs (Gerstberger *et al*, 2014) control messenger RNA (mRNA) expression and coordinate functionally related genes into mRNA regulons (Keene, 2007). These post-transcriptionally controlled networks are more challenging to identify because they may combine the effects of different RBPs or microRNAs on the splicing, polyadenylation, export, stability, localization and translation of mRNA. Dynamic gene expression during development and stress responses, which takes place on a timescale of minutes to hours, requires the coordination of transcriptional and post-transcriptional mechanisms by signalling pathways. The identity of the RBPs that regulate proliferation and differentiation of B cells remains largely unknown.

Polypyrimidine Tract Binding Proteins (PTBP) are RBPs with pleiotropic functions that control alternative splicing (AS), polyadenylation site-selection, mRNA stability and internal ribosome entry site (IRES)-mediated translation (Hu *et al*, 2018; Knoch *et al*, 2004; 2014). They are encoded by a set of highly conserved paralogous genes of which PTBP1 is expressed in many cell types while PTBP2 and PTBP3 (formerly ROD1) are expressed principally in neurons and hematopoietic cells, respectively. Both PTBP1 and

PTBP3 are expressed in mature B cells (Monzon-Casanova *et al*, 2018). PTBP1 can either increase or decrease mRNA stability by binding to the 3'UTR of transcripts, by modulating the AS of exons that will generate transcript isoforms that undergo degradation by nonsense-mediated mRNA decay (NMD) or by affecting polyadenylation site selection and thus the content of the 3'UTR (Hu *et al*, 2018). PTBP1 binds to *Ptbp2* mRNA and, by inducing *Ptbp2* exon 10 skipping, promotes NMD to suppress expression of PTBP2 (Boutz *et al*, 2007).

PTBP1 and PTBP2 have specific and redundant roles and expression of PTBP2 in PTBP1-deficient cells compensates for many functions of PTBP1 (Spellman *et al*, 2007; Vuong *et al*, 2016; Ling *et al*, 2016; Monzon-Casanova *et al*, 2018). To study the unique roles of PTBP1 in B cells, we and others have deleted *Ptbp1* in pro-B cells and found normal B cell development accompanied by upregulated PTBP2 expression but important defects in germinal centre (GC) responses (Monzon-Casanova *et al*, 2018; Sasanuma *et al*, 2019). In GC B cells PTBP1 promotes the selection of B cell clones with high affinity antibodies, in part by promoting the c-MYC gene expression program induced upon positive selection following T cell help, and this function is not compensated by the upregulated PTBP2 (Monzon-Casanova *et al*, 2018). Here we addressed the potential for redundancy between PTBP in B cell development by deleting both *Ptbp1* and *Ptbp2* in pro-B cells. We show that PTBP1 and, in its absence PTBP2, are essential to promote B cell lymphopoiesis beyond the pro-B cell stage. In pro-B cells, PTBP1 suppresses entry into S-phase and promotes transition into mitosis after G2-phase. At the molecular level, PTBP1 controls mRNA abundance and AS of genes important for S-phase entry and mitosis. Therefore, PTBP1 is an essential component of a previously unrecognised posttranscriptional mechanism controlling proliferation in pro-B cells.

Results

PTBP2 can compensate for PTBP1 in B cells

We used a panel of previously characterised PTBP paralog-specific antibodies (Monzon-Casanova *et al*, 2018) to measure the expression of the three main PTBP members at defined stages of B cell development in mouse bone marrow by flow cytometry (**Figures S1B-D**). PTBP1 levels were similar across the different developing B cell populations as the differences we observed in fluorescence intensity for the anti-PTBP1 antibody were also found with the isotype control staining (**Figure S1D**). PTBP2 protein was not detected in any of the B cell developmental stages analysed (**Figures S1C** and **S1D**). PTBP3 was readily detected and also expressed at similar amounts throughout the stages of B cell ontogeny (**Figures S1C** and **S1D**). Thus, PTBP1 and PTBP3, but not PTBP2, are expressed throughout B cell development.

Conditional deletion of a *Ptbp1*-floxed allele in pro-B cells mediated by a $Cd79a^{cre}$ allele ($Cd79a^{cre/+}Ptbp1^{fl/fl}$ mice, denoted here as *Ptbp1* single conditional knock-out, P1sKO) resulted in normal numbers of mature B cells (**Figure 1A** and **1B**) and expression of PTBP2 (Monzon-Casanova *et al*, 2018). Deletion of *Ptbp2* alone with the $Cd79a^{cre}$ allele (P2sKO) had no impact on the number of mature B cells (**Figure 1A**), as expected since PTBP2 is not expressed during B cell development. To establish if PTBP2 compensated for the absence of PTBP1 we generated a double conditional knock-out (dKO) mouse model in which both *Ptbp1* and *Ptbp2* were deleted in pro-B cells using $Cd79a^{cre}$ ($Cd79a^{cre/+}Ptbp1^{fl/fl}Ptbp2^{fl/fl}$ mice, denoted here as P1P2dKO). P1P2dKO mice lacked mature B cells in the spleen and lymph nodes (**Figures 1A**, **1B** and **S1E**). Thus, PTBP1

plays an essential role in the development or maintenance of mature B cells that upon PTBP1 knockout is compensated by upregulation of PTBP2.

The essential role for the PTBPs in B cell development is at the pro-B cell stage

The enumeration of cells at different stages of B cell development in the mouse bone marrow revealed that P1P2dKO mice lacked immature and mature B cells as well as small late pre-B cells (Hardy's FrD) (**Figures 1C** and **1D**). P1P2dKO mice had slightly reduced numbers of FrB and FrC pro-B cells compared to littermate controls (*Cd79a*$^{+/+}$*Ptbp1*$^{fl/fl}$*Ptbp2*$^{fl/fl}$, denoted here as "control" unless stated otherwise) and to *Cd79a*^{cre} "Cre-only" mice (**Figures 1C** and **1D**). In P1P2dKO mice FrC' early pre-B cells, characterised by high expression of CD24 and CD249 (BP-1-positive) were not detected (**Figures 1C** and **1D**). Thus, in the absence of PTBP1 and PTBP2, B cell development is blocked at the pro-B cell stage. P1P2dKO FrB and FrC pro-B cells had higher CD24 staining than control FrB and FrC pro-B cells (**Figure 1C**). Therefore, we set gates (**Figure 1C**) in the P1P2dKO mice to include all of these cells. FrB and FrC pro-B cells from P1P2dKO mice showed increased c-KIT (CD117) staining compared to P1sKO and control pro-B cells and lacked CD2, corroborating a block at an early developmental stage (**Figures S2A** and **S2B**). In P1sKO compared to control and *Cd79a*^{cre} "Cre-only" mice we noticed a ~3-fold increase in the numbers of early-pre-B cells (**Figure 1D**). This increase is the result of higher CD43 staining in P1sKO developing B cells compared to control developing B cells (**Figure 1C**), which leads to the inclusion of more cells in the CD43 high and CD25 low pro- and early pre-B cell gate (**Figure 1D**). We compared P1P2dKO mice to *Rag2*$^{-/-}$ deficient mice (Shinkai *et al*, 1992) in which B cells do not develop past the pro-B cell stage. The numbers of pro-B cells were reduced by ~4.6-fold (FrB) and 19-fold (FrC) in P1P2dKO mice compared to *Rag2*$^{-/-}$ mice (**Figure 1D**). Thus, pro-B cells unable

to recombine their Igh chain locus accumulated in the bone marrow whereas P1P2dKO pro-B cells did not.

To identify early pre-B cells with successfully rearranged Igμ heavy chain we used a staining strategy that included detection of intracellular Igμ (**Figure S2C**). A few early-pre-B cells (B220^{+}, CD19^{+}, IgM^{-}, CD93^{+}, CD43^{high}, Igμ^{+}) were present in P1P2dKO mice, indicating successful recombination of the Igh chain locus in P1P2dKO pro-B cells (**Figure S2C** and **S2D**). However, the numbers of Igμ^{+} early-pre-B cells were decreased by ~13-fold in comparison to control mice (**Figure S2D**). This confirmed the block in B cell development in P1P2dKO mice at the pro-B cell stage. P1P2dKO pro-B cells did not express PTBP1 or PTBP2 protein, demonstrating efficient gene deletion (**Figure S2E**). P1P2dKO pro-B cells expressed increased amounts of PTBP3 compared to pro-B cells from littermate control mice (**Figure S2E**). Taken together, these findings reveal an essential role for PTBP1 in pro-B cells that is compensated for by PTBP2, but not by PTBP3.

PTBP1 regulates mRNA abundance and AS in pro-B cells

To establish the genes regulated by PTBP1 necessary for successful B cell development we carried out mRNAseq on cKIT^{+} FrB pro-B cells from P1P2dKO, P1sKO and control mice (**Figure S3**). To identify transcripts directly bound by PTBP1 we made use of a PTBP1 individual-nucleotide resolution Cross-Linking and ImmunoPrecipitation (iCLIP) dataset (Monzon-Casanova *et al*, 2018) which reveals PTBP1-binding sites in the whole transcriptome and thereby allows distinction between direct and indirect targets. The PTBP1 iCLIP data were from mitogen-activated mouse primary B cells because it was not feasible to purify sufficient numbers of pro-B cells for iCLIP. There is a positive

correlation between the transcriptomes of mitogen-activated primary B cells and pro-B cells (**Figure S4A**), suggesting that the PTBP1 iCLIP data set (**Tables S1** and **S2**) is suitable to infer PTBP1-bound RNAs in pro-B cells.

We analysed changes in mRNA abundance by comparing pro-B cell transcriptomes from the different genotypes in pairwise comparisons (**Figure 2A**). More genes showed differential mRNA abundance when comparing P1P2dKO to control pro-B cells and P1P2dKO to P1sKO pro-B cells than when comparing P1sKO to control pro-B cells (**Figure 2A** and **Table S3**). Almost one-quarter of the genes with increased or decreased mRNA abundance in P1P2dKO pro-B cells encoded transcripts that were directly bound by PTBP1 at the 3'UTR (**Figure S4B** and **Table S3**). The remaining changes observed in mRNA abundance could be attributed to indirect effects, or to roles of PTBP1 in controlling transcript abundance that are independent of 3'UTR binding such as AS leading to NMD (AS-NMD). A striking example of the latter effect is that *Ptbp2* mRNA abundance was increased ~18-fold in P1sKO compared to control pro-B cells (**Figure 2A** and **Table S3**) since *Ptbp2* transcripts in P1sKO pro-B cells included exon 10 and were no longer degraded by NMD.

We used rMATS to compute the differences in exon inclusion levels in pairwise comparisons of the genotypes (Shen *et al*, 2014) (**Figure 2B** and **Table S4**). The inclusion level of a particular alternatively spliced event is displayed as a proportion, scaled to a maximum of 1, of transcripts containing the alternatively spliced mRNA segment. Similar to our observations on mRNA abundance, the absence of both PTBP1 and PTBP2 in pro-B cells resulted in more changes in AS than the absence of PTBP1 (**Figure 2B**). From 30 to 50% of the events with AS changes when comparing P1P2dKO to control pro-B cells

were bound by PTBP1 (**Figure S4D** and **Table S4**), implicating PTBP1 in controlling these events directly. There is a small overlap of genes with changes in mRNA abundance and also AS in the different pairwise comparisons (**Figure 2C**), suggesting that the inclusion of certain exons generates NMD targets. Such AS events promoting NMD will be underestimated in our data, since NMD-targeted isoforms will be degraded and difficult to detect by mRNAseq.

As B cell development is largely unaffected in P1sKO mice, we sought to identify differences in mRNA abundance and AS unique to P1P2dKO pro-B cells compared to both P1sKO and control pro-B cells to identify the changes causing the block in B cell development in the absence of PTBP1 and PTBP2. To this end we carried out unsupervised clustering of the genes with differential mRNA abundance between the different genotypes and genes that were differentially spliced. We identified 1021 and 611 genes with decreased and increased mRNA abundance, respectively, in P1P2dKO compared to control and P1sKO pro-B cells (**Figure 2D**). Amongst AS changes, we found 971 genes with increased or decreased inclusion levels of at least one event in P1P2dKO pro-B cells compared to control and P1sKO (**Figure 2E**). P1P2dKO pro-B cells clustered separately from P1sKO and control pro-B cells when considering abundance changes (**Figure 2D**). When analysing AS, P1P2dKO and P1sKO pro-B cells clustered together but separately from control pro-B cells (**Figure 2E**). Therefore, the compensatory functions of PTBP2 when PTBP1 is absent were more evident when considering mRNA abundance than AS. We observed only 54 genes with different mRNA abundance (cluster d) or changes in AS (clusters i and iii, 384 events) that were predominantly regulated in P1sKO pro-B cells compared to P1P2dKO and control pro-B cells (**Figure 2D** and **2E**). In contrast, large numbers of genes had different mRNA abundance (clusters a, b and c, 1632 genes)

and AS (clusters ii and iv, 1397 events) in P1P2dKO pro-B cells compared to P1sKO and control pro-B cells (**Figure 2D** and **2E**). Therefore, in pro-B cells, PTBP2 has only a few specific targets and mostly compensates for the absence of PTBP1, while PTBP1 ensures the appropriate expression at the level of AS and mRNA abundance of more than 2000 genes.

PTBP1 regulates pathways associated with growth and proliferation

To understand the roles of PTBP1 in B cell development we first inspected mRNA expression of genes important for B cell lymphopoiesis. We found similar mRNA abundance in P1P2dKO compared to control and P1sKO pro-B cells in most of these genes including *Cnot3* (Inoue *et al*, 2015; Yang *et al*, 2016) and *Pax5* (Urbánek *et al*, 1994) (**Figure S4E**). E2A (encoded by *Tcf3*) and IKAROS are two transcription factors with AS (Schjerven *et al*, 2013; Sun & Baltimore, 1991) important for B cell ontogeny. In human, PTBP1 regulates AS of *Tcf3* (Yamazaki *et al*, 2019). We found similar AS patterns of *Ikaros* and *Tcf3* in P1P2dKO compared to control pro-B cells (**Table S4**). *Ebf1* mRNA abundance was reduced ~1.5-fold in P1P2dKO compared to control and P1sKO pro-B cells (**Figure 3A**), but this should not impact B cell development because *Ebf1* haploinsufficiency results in normal B cell ontogeny (Vilagos *et al*, 2012; György *et al*, 2012). *Foxo1* mRNA abundance was reduced ~1.7-fold in P1P2dKO compared to P1sKO and control pro-B cells (**Figure 3A**). PTBP1 bound directly to the 3'UTR of *Foxo1* (**Figure 3B**), indicating a direct role of PTBP1 stabilising *Foxo1* mRNA. *Foxo1* deficient pro-B cells do not develop further and have reduced IL-7 receptor expression (Dengler *et al*, 2008). Indeed, *Il7r* mRNA abundance was reduced ~1.4-fold in P1P2dKO compared to P1sKO and control pro-B cells (**Figure 3A**). However, IL-7 receptor staining was similar between P1P2dKO and control pro-B cells (**Figure 3C**), ruling out a role for a reduction of IL-7 receptor in

the developmental defect of P1P2dKO pro-B cells. FOXO1 promotes RAG expression (Amin & Schlissel, 2008) but *Rag1* and *Rag2* mRNA abundance and AS were unaffected in P1P2dKO pro-B cells (**Figure S4E** and **Table S4**). These data indicate that the known essential elements of the B cell development programme, including three targets of FOXO1, are independent of the PTBPs.

To assess additional cellular pathways affected in the absence of PTBP1 and PTBP2 we carried out gene ontology (GO) enrichment analysis with the genes that showed altered mRNA expression in P1P2dKO compared to P1sKO and control pro-B cells. We analysed genes with increased or decreased mRNA abundance and changes in AS separately (**Figure 3D**). We found numerous enriched GO terms important for the biology of B cells and their progenitors (**Figure 3D** and **Table S5**) such as "antigen processing and presentation of peptide antigen via MHC class II" amongst genes with increased mRNA abundance and "response to lipopolysaccharide" amongst genes with decreased mRNA abundance. "Regulation of neuron differentiation" was enriched amongst genes with reduced abundance and with changes in AS, as we expected from the known roles of PTBPs in neuronal development (Hu *et al*, 2018). Amongst genes with increased mRNA abundance we also found an enrichment for "ribosome biogenesis", "ribonucleoside biosynthetic process" and "rRNA processing", indicating a higher biosynthetic capacity of P1P2dKO pro-B cells compared to control and P1sKO pro-B cells.

Amongst genes with reduced mRNA abundance there was an enrichment for "cyclin-dependent protein serine/threonine kinase inhibitor activity". Cyclin dependent kinase (CDK) inhibitors are major regulators of cell cycle progression (Otto & Sicinski, 2017; Yoon *et al*, 2012) and could be relevant in controlling the proliferation of P1P2dKO pro-

B cells. We found that P1P2dKO FrB pro-B cells had a reduced mRNA abundance of *Cdkn1b*, *Cdkn1c*, *Cdkn2c* and *Cdkn2d* (encoding p27, p57, p18 and p19, respectively) compared to control and P1sKO FrB pro-B cells (**Figure 3E**). None of these CDK inhibitors has an obvious change in AS or a binding site for PTBP1 in the 3'UTR (**Tables S2** and **S4**). FOXO1 promotes p27 expression (Nakamura *et al*, 2000). Therefore, reduced FOXO1 expression (**Figure 3A**) could result in the observed reduced *Cdkn1b* mRNA abundance (**Figure 3E**) in P1P2dKO pro-B cells. Thus, the reduction in mRNA abundance of CDK inhibitors is likely to be an indirect effect of the lack of PTBP1 and PTBP2 at least partly mediated through direct FOXO1 regulation.

PTBP1 represses the entry of pro-B cells into S-phase

The enrichment for CDK inhibitors amongst genes with reduced mRNA abundance and the increased mRNA abundance of biosynthetic pathway components in P1P2dKO compared to P1sKO and controls prompted us to assess the proliferative status of pro-B cells in the P1P2dKO mice. We first assessed the proportions of Fr-B pro-B cells in S-phase by detecting cells that had incorporated EdU for one hour *in vivo* (**Figure S5A**). We found a ~1.6-fold increase in the proportions of FrB pro-B cells in S-phase in P1P2dKO compared to control and P1sKO mice (**Figure S5B**). Moreover, G0/G1 P1P2dKO FrB pro-B cells had increased FSC-A measurements compared to P1sKO and control G0/G1 FrB pro-B cells (**Figure S5C**) which are indicative of an increased cell size and are consistent with a high biosynthetic capacity and a predisposition to enter S-phase.

To understand if the increased proportions of P1P2dKO pro B cells in S-phase were due to an enhanced entry into S-phase or due to an accumulation in S-phase, we sequentially labelled cells *in vivo* with EdU and BrdU (**Figure 4A**). With this approach, we identified

cells in early-, late- or post-S-phase. Cells that incorporated only EdU (post-S-phase) were in S-phase at the beginning, but not at the end of the labelling period; cells that incorporated both EdU and BrdU were in late S-phase; and cells labelled only with BrdU at the end of the labelling period were in early S-phase. In control mice, we detected few pre-pro-B cells in S-phase (3.8% in early- and late-S), compared to 13% of pro-B cells and 53% of early-pre-B cells (**Figures S5D**, **S5E** and **S5F**). In P1P2dKO pro-B cells the proportions of early-S-phase cells were increased 4.7-fold compared to control and 3.2-fold compared to P1sKO pro-B cells (**Figure 4B** and **4C**). The proportions of P1P2dKO pro-B cells in late S-phase and that had exited S-phase (post S-phase) were also increased compared to P1sKO pro-B cells and control pro-B cells (**Figure 4C**). The magnitude of the increase in the proportions of cells in post S-phase was smaller than the increase in either early- or late-S-phase (**Figure 4C**). This indicated that P1P2dKO pro-B cells enter S-phase more readily than control pro-B cells but they fail to progress through S-phase at the same pace as PTBP1-sufficient pro-B cells.

PTBP1 promotes the entry of pro-B cells into mitosis

To look for possible additional effects of PTBP1 upon the G2/M-phases of the cell cycle we analysed DNA synthesis in combination with DNA content (**Figure 4D**). Compared to control and P1sKO, P1P2dKO pro-B cells in G2/M-phase were increased both in proportion (~40-fold) and number (~8-fold) (**Figure 4E**). These findings were confirmed when identifying FrB pro-B cells using cell surface markers ($CD19^+$, $CD24^+$, $CD249^-$, $CD2^-$, $CD25^-$, IgM^-, IgD^-) (**Figure S5A** and **S5B**). To distinguish G2 and M phases of the cell cycle we stained FrB pro-B cells both for DNA and phosphorylated histone 3 (pH3) which marks cells in mitosis (**Figure 4F**). The proportion of pH3-positive cells amongst P1P2dKO FrB pro-B cells with 4N-DNA content was reduced ~3-fold compared

to the proportions found amongst P1sKO and control FrB pro-B cells (**Figure 4G**). Therefore, the majority of P1P2dKO pro-B cells with 4N-DNA content were in G2-phase and had not entered mitosis. PTBP1, and in its absence PTBP2, were thus required for pro-B cells to progress from G2 to M-phase of the cell cycle.

PTBP1 controls CDK activity in pro-B cells

The decrease in mRNA abundance of CDK inhibitors (**Figure 3E**) and the abnormal proliferation observed in pro-B cells due to the absence of PTBP1 and PTBP2 (**Figure 4**) prompted us to measure expression of the CDK inhibitor p27 in the different phases of the cell cycle. We found p27 staining reduced ~1.7-fold in G0/G1 P1P2dKO FrB pro-B cells compared to G0/G1 P1sKO and control FrB pro-B cells (**Figure 5A** and **5B**), consistent with the decreased *Cdkn1b* mRNA abundance in FrB pro-B cells (**Figure 3E**). In contrast, in G2 cells p27 staining was increased ~7-fold in P1P2dKO FrB pro-B cells compared to P1sKO and control FrB pro-B cells (**Figure 5A** and **5B**). p27 expression is regulated at the post-translational level as well as the transcriptional level (Vervoorts & Lüscher, 2008). Moreover, PTBP1 promotes p27 IRES-mediated translation directly in human cells (Cho *et al*, 2005). We did not find mouse PTBP1 bound to the *Cdkn1b* 5'UTR (**Table S2**) although *Cdkn1b* mRNA is expressed in mitogen-activated B cells. Thus, additional layers of regulation are expected to contribute to the dynamic regulation of p27 protein abundance across the different phases of the cell cycle observed in the absence of PTBP1 and PTBP2.

In addition to p27 expression, we assessed CDK activity by measuring the extent of RB phosphorylation in Ser-807/811, which is mediated in G1 by CDKs and promotes the entry into S-phase (Otto & Sicinski, 2017), and of SAMHD1 phosphorylation in Thr-592,

which is a surrogate marker for CDK1 activity (Cribier *et al*, 2013). Proportions of both p-RB and p-SAMHD1-positive cells were increased amongst P1P2dKO G0/G1 FrB pro-B cells compared to control and P1sKO G0/G1 FrB pro-B cells (**Figure 5C** and **5D**), indicating an abnormally high CDK activity in G0/G1 P1P2dKO pro-B cells. In contrast, amongst pro-B cells in G2/M-phases the proportions of p-RB and p-SAMDH1-positive cells were reduced in P1P2dKO mice compared to control and P1sKO mice (**Figure 5C** and **5D**). This indicates a requirement for PTBP1 to achieve sufficient CDK1 activity to enter mitosis. Thus, PTBP1 is essential for controlling the activity of CDKs in different phases of the cell cycle in pro-B cells, to limit entry into S-phase and to promote entry into mitosis.

PTBP1 controls the expression of S-phase entry regulators in pro-B cells

GO enrichment analysis of genes differentially expressed in P1P2dKO compared to control and P1sKO pro-B cells identified an enrichment for ribosome biogenesis and CDK inhibitors but it did not detect further terms directly related with proliferation. Therefore to identify PTBP1 targets directly implicated in the progression through different phases of the cell cycle we assessed changes in mRNA abundance of genes known to be highly expressed specifically in the S and G2/M-phases (Giotti *et al*, 2018) between FrB pro-B cells of the different genotypes. S- and G2/M-associated transcripts were not globally increased in P1P2dKO FrB pro-B cells compared to control and P1sKO FrB pro-B cells (**Figure 6A** and **Table S6**). This indicates that the majority of the changes observed in the transcriptome of P1P2dKO compared to control and P1sKO pro-B cells are not the result of comparing populations with different proliferative status, but are reflective of an altered pro-B cell transcriptome. Thus, instead of gene sets, it was possible that individual genes with rate limiting properties for cell cycle progression, which could also control the expression of

CDK-inhibitors and CDK activities, were directly regulated by PTBP1. Therefore, we considered further genes affected in the absence of PTBP1 and PTBP2 but not in the absence of PTBP1 alone that are known to regulate the cell cycle.

We identified four genes associated with S-phase entry with direct PTBP1 binding and changes at the levels of mRNA abundance and AS. Two genes (*Myc* and *Ccnd2*) whose proteins promote entry into S-phase, showed increased mRNA abundance in P1P2dKO compared to P1sKO and control pro-B cells (**Figure 6B**). Two further genes (*Btg2* and *Rbl1*), whose proteins inhibit S-phase entry, had reduced mRNA abundance in P1P2dKO compared to control and P1sKO FrB pro-B cells (**Figure 6B**). PTBP1 bound to the 3'UTR of *Myc* (**Figure S6**) and we confirmed an increase of c-MYC protein abundance in G0/G1 P1P2dKO FrB pro-B cells compared to control and P1sKO G0/G1 FrB pro-B cells (**Figure 6C** and **6D**) as the fold-change increase in fluorescence intensity of the c-MYC staining (2.2-fold) was greater than the fold-change increase in fluorescence intensity of the control staining (1.5-fold). Therefore, in pro-B cells PTBP1 suppresses *Myc*.

CYCLIN-D2 pairs with CDK4/6 and promotes entry into S-phase (Otto & Sicinski, 2017). *Ccnd2* abundance (encoding CYCLIN-D2) was increased ~2-fold in P1P2dKO compared to control and P1sKO FrB pro-B cells (**Figure 6B**) and PTBP1 bound to the *Ccnd2* 3'UTR (**Figure S6**). c-MYC induces transcription of *Ccnd2* (Bouchard *et al*, 2001). Therefore, PTBP1 and PTBP2 could reduce *Ccnd2* mRNA abundance indirectly by suppressing c-MYC-mediated transcription and directly by binding its mRNA.

BTG2 inhibits G1 to S transition and promotes B cell development by suppressing proliferation in late-pre-B cells (Dolezal *et al*, 2017). *Btg2* mRNA abundance was reduced

~2-fold due to *Ptbp1* and *Ptbp2* deletion (**Figure 6B**). No obvious change in *Btg2* AS was detected but PTBP1 binding sites were present at the *Btg2* 3'UTR (**Figure S6**). Therefore, PTBP1 could directly promote BTG2 expression in pro-B cells by stabilising *Btg2* transcripts.

p107 (encoded by *Rbl1*) represses E2F transcription factors and entry into S-phase (Bertoli *et al*, 2013). *Rbl1* mRNA abundance was reduced ~1.5-fold in P1P2dKO compared to control and P1sKO pro-B cells (**Figure 6B**). PTBP1 and PTBP2 suppress the inclusion of a downstream alternative 5' splice site (A5SS) in *Rbl1* exon 8. Use of this A5SS in P1P2dKO pro-B cells generates an NMD-target isoform (**Figure 6E**). PTBP1 binds to adjacent regions of this alternatively spliced event (**Figure 6E**). This A5SS event is conserved in human, as PTBP1- and PTBP2-depleted HeLa cells (Ling *et al*, 2016) also have an increased usage of the downstream A5SS compared to PTBP-sufficient cells, resulting in reduced *RBL1* mRNA abundance (**Figure 6F** and **6G**). Therefore, PTBP1 promotes *Rbl1* expression by suppressing production of the NMD-targeted *Rbl1* isoform. Collectively, deregulated expression of *Myc*, *Ccnd2*, *Btg2* and *Rbl1* in the absence of PTBP1 and PTBP2 would act to drive entry of pro-B cells into S-phase.

PTBP1 promotes expression of a network of mitotic factors via AS

We also identified transcripts important for the transition from G2 to M-phase with altered expression in P1P2dKO pro-B cells (**Figure 6A**). The abundance of *Cdc25b*, *Ect2, Kif2c* and *Kif22* was reduced (~3, ~5, ~2 and ~2-fold, respectively) in P1P2dKO compared to control and P1sKO FrB pro-B cells (**Figure 7A**). CDC25B is a phosphatase promoting G2/M transition by activating CDK1 (Boutros *et al*, 2007). *Cdc25b* AS was unaffected by PTBP1 and PTBP2 absence but PTBP1 bound to the *Cdc25b* 3'UTR (**Table**

S4 and **Figure S6**). Thus, PTBP1 probably promotes *Cdc25b* expression by binding to its 3'UTR and enhancing its stability.

There were three genes (*Ect2*, *Kif2c* and *Kif22*) whose changes in mRNA abundance could be explained by AS events leading to NMD. ECT2 controls spindle formation in mitosis by exchanging GDP for GTP in small GTPases such as RhoA (Yüce *et al*, 2005). In P1P2dKO pro-B cells an *Ect2* alternative exon with two alternative 3'SS was found more frequently included compared to P1sKO and control pro-B cells (**Figure 7B**). Inclusion of this AS exon, using either of the two alternative 3'SS, will generate transcripts predicted to be degraded by NMD. PTBP1 bound nearby this NMD-triggering exon (**Figure 7B**) where it is predicted to suppress exon inclusion (Llorian *et al*, 2010) promoting high *Ect2* mRNA levels in pro-B cells.

KIF2c (MCAK) and KIF22 (KID) are two kinesin motor family members that transport cargo along microtubules during mitosis (Cross & McAinsh, 2014). Both have increased inclusion of an exon that generates predicted NMD-targets in P1P2dKO compared to P1sKO and control pro-B cells and some evidence for PTBP1 binding in adjacent regions (**Figure 7B**). These data showed that PTBP1 promoted expression of genes important for mitosis by suppressing AS linked to NMD (*Ect2*, *Kif2c*, *Kif22*) and by stabilizing mRNA (*Cdc25b*). The altered expression of these genes in the absence of PTBP1 and PTBP2 is likely to contribute to the high proportions of G2 cells observed in P1P2dKO pro-B cells.

Taken together, our findings implicate PTBP1 as a regulator of the cell cycle in pro-B cells. PTBP1 is essential to control appropriate expression of an mRNA regulon dictating CDK activity, progression to S-phase and entry into mitosis (**Figure 7C**). In the absence of

PTBP1 and its partially redundant paralog PTBP2, the molecular control of the cell cycle in primary pro-B cells is disrupted and B cell development is halted.

Discussion

Here we present an essential role for PTBP1 in controlling B cell development that can be compensated for by PTBP2. Combined PTBP1 and PTBP2 deficiency resulted in a complete block in B cell development and striking defects at two stages of the cell cycle of pro-B cells. The enhanced entry into S-phase of pro-B cells lacking PTBP1 and PTBP2 was unanticipated since in other systems, including GC B cells, PTBP1 promoted proliferation (Suckale *et al*, 2011; Shibayama *et al*, 2009; La Porta *et al*, 2016) and progression through late S-phase (Monzon-Casanova *et al*, 2018). These previous studies were done in the presence of PTBP2 (Suckale *et al*, 2011; Shibayama *et al*, 2009; La Porta *et al*, 2016) and GC B cells did not tolerate deletion of both PTBP1 and PTBP2 (Monzon-Casanova *et al*, 2018). Thus, our findings may not be unique to pro-B cells and may be found in other cell types if they survive the absence of PTBP1 and PTBP2 long enough to assess cell-cycle progression.

Although the absence of PTBP1 and PTBP2 caused qualitative and quantitative changes in mRNA expression of many genes, we found that PTBP1 bound and controlled the abundance and splicing of a collection of mRNAs that together comprise a cell cycle mRNA regulon. The proteins encoded within this mRNA regulon interact with each other to generate feed-forward activation loops that promote cell cycle entry and mitosis. For example, c-MYC suppresses *Cdkn1b* (encoding p27) (Yang *et al*, 2001) and increases *Ccnd2* transcription (Bouchard *et al*, 2001). CYCLIN-D2 promotes nuclear export and degradation of p27/CDKN1b (Susaki *et al*, 2007) and p27 directly inhibits CYCLIN-D-CDK4/6 complexes (Yoon *et al*, 2012). Although the block in G2-phase we observed could have resulted from a response to DNA damage we found little evidence for enhanced DNA

damage in FrB pro-B cells (data not shown). This data suggested that the block at G2 in P1P2dKO pro-B cells resulted mainly from increased p27 expression. The net outcome from deregulation of the PTBP1 controlled cell cycle mRNA regulon in the absence of PTBP1 and PTBP2 is an enhanced CDK activity in G0/G1 pro-B cells that drives entry into S-phase and a reduced CDK activity amongst blocked G2 pro-B cells.

The molecular mechanisms of PTBP action on the cell cycle mRNA regulon that we assessed were limited to the regulation of AS and mRNA abundance. PTBPs are known, in addition, to control polyadenylation site choice and IRES-mediated translation of certain transcripts (Hu *et al*, 2018). Therefore, we can expect that additional roles for PTBP1 regulating translation efficiencies and polyadenylation site usage in pro-B cells may emerge. Moreover, by suppressing the inclusion of non-conserved cryptic exons that generate NMD targets (Ling *et al*, 2016; Sibley *et al*, 2016), PTBPs may play a broader role in maintaining the global "fidelity" of the transcriptome. Cryptic exons, that are poorly conserved between mouse and human have been found when both PTBP1 and PTBP2 were depleted (Ling *et al*, 2016). In pro-B cells deficient for PTBP1 and PTBP2 we found cryptic exons promoting mRNA degradation amongst cell cycle regulators. For most of them we did not find evidence for their conservation in human cells where PTBP1 and PTBP2 were absent (Ling *et al*, 2016). However, the A5SS in *Rbl1* that generates an NMD-target was conserved in human, suggesting that it is a functional AS-NMD event with a role in post-transcriptional control.

The role that we have found here for PTBP1 and PTBP2 is distinct from that of other RBPs such as AUF1 (Sadri *et al*, 2010) and ELAVL1 (Diaz-Muñoz *et al*, 2015) which, when deleted, have little effect on B cell development. The ZFP36 family members ZFP36L1 and

ZFP36L2 are important for quiescence during lymphocyte development, but their absence has a much milder impact on B cell development (Galloway *et al*, 2016) than does the combined absence of PTBP1 and PTBP2. The unique role that we have found for PTBP1 in controlling the cell cycle, and its redundancy with PTBP2, further underscores the importance of post-transcriptional RNA regulation as an essential component of the molecular regulation of the cell cycle. In the context of B cells this regulation is essential for developmental progression beyond the pro-B cell stage.

Methods

Mice

Mice were bred and maintained in the Babraham Institute Biological Support Unit. Since the opening of this barrier facility (2009), no primary pathogens or additional agents listed in the FELASA recommendations have been confirmed during health monitoring surveys of the stock holding rooms. Ambient temperature was ~19-21°C and relative humidity 52%. Lighting was provided on a 12 hour light: 12 hour dark cycle including 15 min 'dawn' and 'dusk' periods of subdued lighting. After weaning, mice were transferred to individually ventilated cages with 1-5 mice per cage. Mice were fed CRM (P) VP diet (Special Diet Services) ad libitum and received seeds (e.g. sunflower, millet) at the time of cage-cleaning as part of their environmental enrichment. All mouse experimentation was approved by the Babraham Institute Animal Welfare and Ethical Review Body. Animal husbandry and experimentation complied with existing European Union and United Kingdom Home Office legislation and local standards. All mice were used experimentally between 8 and 15 weeks of age and were age- and sex-matched within experiments, although no sex-associated differences were observed in the results obtained. Conditional knockout mice used were derived from crossing the following transgenic strains: *Ptbp1*$^{fl/fl}$ (Ptbp1^{tm1Msol}) (Suckale *et al*, 2011), *Ptbp2*$^{fl/fl}$ (Ptbp2$^{tm1.1Dblk}$) (Li *et al*, 2014) and *Cd79a*^{cre} (Cd79a$^{tm1(cre)Reth}$) (Hobeika *et al*, 2006). *Rag2*$^{-/-}$ knockout mice (Shinkai *et al*, 1992) (Rag2^{tm1Fwa}) were also used. All mice were on the C57BL/6 background.

In vivo EdU and BrdU administration

In EdU-only and in EdU and BrdU double-labelling experiments 1 to 5 mice of different genotypes and the same sex were kept in individually ventilated cages. Whenever possible females were used as this allowed for a higher number of mice with different genotypes per cage. Males and females showed the same phenotypes observed due to PTBP absence. In EdU-only labelling experiments mice were injected with 1 mg EdU (5-ethynyl-2'-deoxyuridine, cat #E10415, ThermoFisher Scientific) intraperitoneally and were killed one hour after injection. In EdU and BrdU (5-bromo-2′-deoxyuridine, cat# B5002-500mg, Sigma) labelling experiments mice were injected first with 1 mg EdU (cat #E10415, ThermoFisher Scientific) intraperitoneally. One hour later, the same mice were injected with 2 mg BrdU and the mice were killed 1 hour and 40 minutes after the injection with EdU.

Flow cytometry

Single cell suspensions were prepared from spleens and lymph nodes by passing the organs through cell strainers with 70 µm and 40 µm pore sizes in cold RPMI-1640 (cat# R8758, Sigma) with 2% fetal calf serum (FCS). Single cell suspensions from bone marrow were prepared by flushing the marrow from femurs and tibias and passing the cells through a cell strainer with 40 µm pore size in cold RPMI-1640 with 2%FCS. Fc receptors were blocked with monoclonal rat antibody 2.4G2. Cells were stained with combinations of antibodies listed in **Table S7**. Cell surface staining was carried out for 45 minutes on ice by incubating cells with a mixture of antibodies in cold FACS buffer (PBS +0.5%FCS). For intracellular staining, cells were fixed with Cytofix/Cytoperm™ Fixation and Permeabilization Solution (cat# 554722, BD) on ice, washed with FACS Buffer and frozen in 10% DMSO 90% FCS at -80°C at least overnight. After thawing, cells were washed with FACS Buffer and re-fixed with Cytofix/Cytoperm™ Fixation and Permeabilization

Solution (cat# 554722, BD) for 5 minutes on ice. Cells were washed with Perm/Wash Buffer (cat# 554723, BD) and intracellular staining with antibodies was carried out by incubating fixed and permeabilized cells in Perm/Wash Buffer (cat# 554723, BD) first with monoclonal rat antibody 2.4G2 and subsequently with the desired antibodies in Perm/Wash Buffer at room temperature. EdU was detected with Click-iT™ Plus EdU kits (cat# C10646, for AF594 and cat# C10636 for pacific blue, ThermoFisher Scientific). For double detection of EdU and BrdU, cells were treated as for intracellular staining but, before adding the intracellular antibodies, cells were treated with TURBO™ DNase (12 units/10^7 cells, cat# AM2239, ThermoFisher Scientific) for 1 hour at 37°C. Subsequently, EdU was detected with the Click-iT™ reaction following the instructions from the manufacturer. Cells were washed with Perm/Wash Buffer (cat# 554723, BD) and incubated with anti-BrdU-AF647 antibody (MoBU-1, cat# B35133, ThermoFisher Scientific). DNA was stained in the last step before flow cytometry analysis with 7AAD in EdU and BrdU double-labelling experiments or with Vybrant™ DyeCycle™ Violet Stain in experiments where no DNA-digestion was carried out (cat # V35003, ThermoFisher Scientific). Flow cytometry data were acquired on a BD LSRFortessa with 5 lasers and was analysed using FlowJo software (versions 10.6.0 and 10.0.8r1).

mRNAseq libraries from FrB pro-B cells

FrB c-KIT+ pro-B cells ($B220^+$, $CD19^+$, IgD^-, IgM^-, $CD2^-$, $CD25^-$, $CD43^{high}$, $cKIT^+$, $CD24^+$ and $CD249^-$) were sorted from bone marrow cells isolated from femurs and tibias. Bone marrow cells from 4-6 mice of the same genotype and sex were pooled and depleted of unwanted cells with anti Gr-1 (RB6-8C5), CD11b (M1/70), IgD (11-26c.2a), NK1.1 (PK136), CD3e (145-2C11) and Ter119 biotinylated antibodies and anti-biotin microbeads (cat# 130-090-485, Miltenyi) before sorting. The sorting strategy for FrB

pro-B cells is shown in **Figure S3**. RNA from 15,000 to 200,000 FrB cells was isolated with the RNeasy Micro Kit (cat# 74004, Qiagen). mRNAseq libraries were prepared from 5 biological replicates per genotype: (three genotypes: ctrl (*Cd79a*$^{+/+}$*Ptbp1*$^{fl/fl}$*Ptbp2*$^{fl/fl}$), P1sKO (*Cd79a*$^{cre/+}$*Ptbp1*$^{fl/fl}$*Ptbp2*$^{+/+}$) and P1P2dKO (*Cd79a*$^{cre/+}$*Ptbp1*$^{fl/fl}$*Ptbp2*$^{fl/fl}$); three samples from females and two samples from males per genotype) by generating cDNA from 2 ng RNA and 9 PCR cycles per replicate with the SMART-Seq® v4 Ultra® Low Input RNA Kit for Sequencing (cat# 634891, Takara) and by enzymatic fragmentation of 300 pg of cDNA followed by 12 PCR cycles using the Nextera XT DNA Library Preparation Kit (cat# FC-131-1096, Illumina). Sequencing of the 15 mRNAseq libraries multiplexed together was carried out with an Illumina HiSeq2500 on a 2x125 bp paired-end run.

PTBP1 iCLIP

PTBP1 iCLIP was carried out previously from mitogen-activated B cells (splenic B cells stimulated with LPS for 48 hours) (Monzon-Casanova *et al*, 2018). The data generated were re-analysed to map reads using a splicing-aware software. Reads from five PTBP1 iCLIP libraries were mapped to the GRCm38.p5 mouse genome from Gencode with STAR (v 2.5.4b) (Dobin *et al*, 2013). Reads were de-duplicated using random barcodes included in the library preparation and xlink-sites (**Table S1**) and clusters of binding (**Table S2**) were identified with iCount https://icount.readthedocs.io/en/latest/cite.html as previously described (Monzon-Casanova *et al*, 2018). Detection of a binding site with iCLIP (König *et al*, 2010) is highly dependent on the abundance of the RNA, therefore all replicates were pooled together to identify xlink sites and clusters of binding. Xlink sites and clusters of PTBP1 binding were assigned to transcripts and genomic features with the following hierarchy: CDS, 3'UTR, 5'UTR, intron, ncRNA using the Mus_musculus.GRCm38.93.gtf annotation from Ensembl (**Tables S1** and **S2**).

mRNA abundance analysis

mRNAseq libraries were trimmed with Trim Galore (v 1.15 https://www.bioinformatics.babraham.ac.uk/projects/trim_galore/) with default parameters and mapped with Hisat2 (v 2.1.0) (Kim *et al*, 2015) with -p 7 -t --phred33-quals --no-mixed --no-discordant parameters, the Mus_musculus.GRCm38 genome and known splice sites from the Mus_musculus.GRCm38.90 annotation. Read counts mapped over genes were counted with HTSeq (v0.10.0) (Anders *et al*, 2015) with f bam -r name -s no -a 10 parameters and the Mus_musculus.GRCm38.93.gtf annotation from Ensembl. Reads mapping to immunoglobulin genes (including V, D, J gene segments, light and heavy immunoglobulin genes and T cell receptor genes) were excluded before DESeq2 analysis. Differences in mRNA abundance were computed with DESeq2 (v1.22.1) (Love *et al*, 2014) by extracting differences between different genotypes in pair-wise comparisons using "apeglm" method as a shrinkage estimator (Zhu *et al*, 2019). Information on the sex of the mice from which the mRNAseq libraries were generated was included in the design formula in addition to the genotype (design = ~ Sex + Genotype). From the DESeq2 results we only considered genes with a mean expression level of at least 1 FPKM (from the five biological replicates) in any of the three genotypes analysed. FPKMs were calculated with cuffnorm from Cufflinks (v2.2.1) (Trapnell *et al*, 2012) using the -library-norm-method geometric. We considered genes with differential mRNA abundance as those with a |log2-fold change| >0.5 and a p-adjusted value of <0.05 (**Table S3**).

A gene with different mRNA abundance was bound by PTBP1 at the 3'UTR if at least one cluster of PTBP1-binding from the PTBP1 iCLIP data (**Table S2**) was found to overlap

with any 3'UTRs annotated in the Mus_musculus.GRCm38.93.gtf for that gene after assignation to genomic features for the binding sites of the iCLIP as described above.

Genes with different mRNA abundance in P1P2dKO FrB pro-B cells compared to P1sKO and control FrB cells (**Figure 2D** and **Table S5**) were identified after hierarchical clustering of the Euclidian distances between Z-scores of each gene calculated from the DESeq2 normalised read counts for the 15 mRNAseq libraries (5 biological replicates per genotype). Genes with different mRNA abundance in any of the three pairwise comparisons carried out (**Figure 2A**) were considered in the hierarchical clustering.

Alternative splicing analysis

Trimmed reads generated by Trim Galore were further trimmed to 123 bp and reads which were smaller than 123 bp were discarded with Trimmomatic (v0.35) (Bolger *et al*, 2014) in order to obtain only pairs of reads 123 bp long. 123 bp-long reads were mapped to the Mus_musculus.GRCm38 genome as described above, but only uniquely-mapped reads were kept by using the -bS -F 4 -F 8 -F 256 -q 20 parameters in samtools when converting hisat2 sam files to bam files. rMATS (Turbo v4.0.2) (Shen *et al*, 2014) was run with the -t paired --readLength 123 parameters and the Mus_musculus.GRCm38.93.gtf annotation for each individual pairwise comparison. Only results from rMATS with reads on exon-exon junctions were considered further. Significantly differential alternative splicing events (**Table S4**) were defined as events that have an FDR<0.05, have an absolute inclusion level difference >0.1 (to reduce the number of significant (FDR <0.05) differentially spliced events computed by rMATS with small changes in splicing between the different pairwise comparisons), come from genes expressed with at least 1 FPKM (mean across five biological replicates in any of the genotypes analysed) and have at least

80 reads from the sum of the five biological replicates mapping to either the included or skipped alternative splicing event in at least one of the two conditions analysed. Only alternative splicing events with the highest inclusion level difference were kept out of AS events which had the same genomic coordinates in the AS event (**Table S4**). rMATS considers five different types of alternative splicing events: skipped exons (SE), mutually exclusive exons (MXE), alternative 5' and 3' splice sites (A5SS and A3SS, respectively) and retained introns (RI) (**Figure S4C**). Proportions of differential alternative splicing events were defined as bound by PTBP1 (**Figure S4D**, **Table S4**) with different criteria depending on the type of AS event.

An SE was bound by PTBP1 if PTBP1 clusters (**Table S2**) were found on the SE, 500 nucleotides upstream or downstream of the AS SE, on either of the constitutive flanking exons or in 500 nucleotides downstream or upstream of the upstream and downstream constitutive exons, respectively. An A5SS was bound if PTBP1 clusters were found on the longest exon containing the A5SS, on the downstream intronic 500 nucleotides of the A5SS, on the downstream constitutive flanking exon or the 500 intronic nucleotides upstream of the downstream constitutive flanking exon. An A3SS was bound by PTBP1 if PTBP1 clusters were found on the longest exon containing the A3SS, the 500 intronic nucleotides upstream of the A3SS, the upstream constitutive flanking exon or the 500 intronic nucleotides downstream of the upstream constitutive flanking exon. An MXE was bound by PTBP1 if PTBP1 clusters were found on either MXE, the upstream or downstream 500 intronic nucleotides of either MXE, the upstream or downstream constitutive flanking exons or the downstream or upstream 500 intronic nucleotides from the upstream or downstream constitutive flanking exons, respectively. A RI was

bound by PTBP1 if PTBP1 clusters were found on the RI or on either constitutive flanking exon.

Differentially alternative splicing events in P1P2dKO FrB pro-B cells compared to control and P1sKO FrB pro-B cells (**Figure 2E**) were identified by hierarchical clustering using complete linkage clustering of the Euclidean distances between Z-scores of each AS event calculated from the rMATS inclusion levels for the 15 mRNAseq libraries (5 biological replicates per genotype). AS events found in any of the three pairwise comparisons (**Figure 2B**) were used in the hierarchical clustering.

Gene ontology term enrichment analysis

Genes belonging to different clusters based on differences in mRNA abundance or AS patterns between the P1P2dKO FrB pro B cells and the other genotypes (P1sKO and Controls) (**Figures 2D**, **2E** and **Table S5**) were used for gene ontology enrichment analysis with GOrilla (Eden *et al*, 2009). Genes expressed with a mean of least 1 FPKM across the 5 biological replicates in any of the genotypes were used as background list for expressed genes in FrB pro-B cells. **Figure 2D** shows representative enriched terms selected amongst closely related GO terms by manual inspection of the ontology. **Table S5** is a full list of all enriched GO enriched terms. Representative selected terms are highlighted.

Comparison of transcriptomes from pro-B cells and mitogen activated B cells

Transcriptomes from control FrB pro-B cells and mitogen-activated primary B cells (LPS for 48 hours) (Diaz-Muñoz *et al*, 2015) were compared by calculating Spearman's rank correlation of the Log mean TPM (Transcripts per million reads) for each gene. Mean

TPMs were calculated in FrB pro-B cells from five biological replicates and in mitogen-activated B cells from four biological replicates. TPMs were calculated after counting reads mapping to genes with HTSeq and the Mus_musculus.GRCm38.93.gtf annotation from Ensembl.

mRNAseq from human PTBP1 and PTBP2 depleted HeLa

Sequences from control and mRNAseq libraries where PTBP1 and PTBP2 were knocked down in HeLa cells by Ling et al. (Ling *et al*, 2016) were trimmed with Trim Galore (v 0.6.2_dev) and mapped with Hisat2 (v 2.1.0) (Kim *et al*, 2015) with --dta --sp 1000,1000 -p 7 -t --phred33-quals --no-mixed --no-discordant parameters, the Homo_sapiens.GRCh38 genome annotation and a file with known splice sites generated from the Homo_sapiens.GRCh38.87 annotation. Mapped reads were counted with HTSeq (v0.10.0) (Anders *et al*, 2015) with -f bam -r name -s no -a 10 parameters and the Homo_sapiens.GRCh38.93.gtf annotation from Ensembl. Read counts were normalised with DESeq2 (Love *et al*, 2014) (v 1.20.0).

Statistical analysis

Statistical analysis of flow cytometry data was carried out with GraphPad Prism version 7.0e. Details of tests carried out are found in the legends. Statistical analysis of mRNAseq data was carried out as described in the "mRNA abundance analysis" and "Alternative splicing analysis" sections.

Data availability

mRNAseq libraries and iCLIP analysis generated in this study have been deposited in GEO and can be accessed with the GSE136882 accession code at GEO. Mitogen-activated

primary B cell mRNAseq libraries were previously reported and can be accessed with the GSM1520115, GSM1520116, GSM1520117and GSM1520118 accession codes in GEO.

Author contributions

E.M.C., M.T. and C.W.J.S. designed experiments. E.M.C. and K.T. performed experiments and analysed data. E.MC., L.S.M. and K.Z. designed and carried out computational analysis. E.M.C. and M.T. wrote the manuscript with input from the co-authors.

Acknowledgments

We thank Douglas L. Black for the *Ptbp2*$^{fl/fl}$ mice, Michael Reth for the *Cd79a*^{cre} mice, Frederick W. Alt for the *Rag2*$^{-/-}$ mice and Michele Solimena for the *Ptbp1*$^{fl/fl}$ mice and the anti-PTBP2 antibody; Kirsty Bates, Arthur Davis, Attila Bebes, Simon Andrews, the Babraham Institute Biological Support Unit, Flow Cytometry and Bioinformatics Facilities for technical assistance; Tony Ly, Anne Corcoran, Geoff Butcher, Daniel Hodson and members of the Turner, Smith and Zarnack laboratories for helpful discussions. This study was supported by funding from the Biotechnology and Biological Sciences Research Council (BBSRC) (BB/J00152X/1; BB/P01898X/1; BBS/E/B/000C0407; and BBS/E/B/000C0427 and the BBSRC Core Capability Grant to the Babraham Institute), a Wellcome Investigator (200823/Z/16/Z) award to M.T and a Short Term Scientific Mission Award to E.M.C. from the European Cooperation in Science and Technology action CA17103, “Delivery of Antisense RNA Therapeutics”.

Competing interests

The authors declare no competing financial interests.

References

Amin RH & Schlissel MS (2008) Foxo1 directly regulates the transcription of recombination-activating genes during B cell development. *Nat. Immunol.* **9:** 613–622

Anders S, Pyl PT & Huber W (2015) HTSeq--a Python framework to work with high-throughput sequencing data. *Bioinformatics* **31:** 166–169

Bertoli C, Skotheim JM & de Bruin RAM (2013) Control of cell cycle transcription during G1 and S phases. *Nature Reviews Molecular Cell Biology* **14:** 518–528

Bolger AM, Lohse M & Usadel B (2014) Trimmomatic: a flexible trimmer for Illumina sequence data. *Bioinformatics* **30:** 2114–2120

Bouchard C, Dittrich O, Kiermaier A, Dohmann K, Menkel A, Eilers M & Lüscher B (2001) Regulation of cyclin D2 gene expression by the Myc/Max/Mad network: Myc-dependent TRRAP recruitment and histone acetylation at the cyclin D2 promoter. *Genes Dev.* **15:** 2042–2047

Boutros R, Lobjois V & Ducommun B (2007) CDC25 phosphatases in cancer cells: key players? Good targets? *Nature Reviews Cancer 2017 17:2* **7:** 495–507

Boutz PL, Stoilov P, Li Q, Lin C-H, Chawla G, Ostrow K, Shiue L, Ares M & Black DL (2007) A post-transcriptional regulatory switch in polypyrimidine tract-binding proteins reprograms alternative splicing in developing neurons. *Genes Dev.* **21:** 1636–1652

Busslinger M (2004) Transcriptional Control of Early B Cell Development1. *http://dx.doi.org/10.1146/annurev.immunol.22.012703.104807* **22:** 55–79

Cho S, Kim JH, Back SH & Jang SK (2005) Polypyrimidine Tract-Binding Protein Enhances the Internal Ribosomal Entry Site-Dependent Translation of p27Kip1 mRNA and Modulates Transition from G1 to S Phase. *Mol. Cell. Biol.* **25:** 1283–1297

Clark MR, Mandal M, Ochiai K & Singh H (2014) Orchestrating B cell lymphopoiesis through interplay of IL-7 receptor and pre-B cell receptor signalling. *Nature Reviews Immunology* **14:** 69–80

Cribier A, Descours B, Valadão ALC, Laguette N & Benkirane M (2013) Phosphorylation of SAMHD1 by Cyclin A2/CDK1 Regulates Its Restriction Activity toward HIV-1. *Cell Reports* **3:** 1036–1043

Cross RA & McAinsh A (2014) Prime movers: the mechanochemistry of mitotic kinesins. *Nature Reviews Molecular Cell Biology* **15:** 257–271

Dengler HS, Baracho GV, Omori SA, Bruckner S, Arden KC, Castrillon DH, DePinho RA & Rickert RC (2008) Distinct functions for the transcription factor Foxo1 at various stages of B cell differentiation. *Nat. Immunol.* **9:** 1388–1398

Diaz-Muñoz MD, Bell SE, Fairfax K, Monzon-Casanova E, Cunningham AF, Gonzalez-Porta M, Andrews SR, Bunik VI, Zarnack K, Curk T, Heggermont WA, Heymans S, Gibson GE, Kontoyiannis DL, Ule J & Turner M (2015) The RNA-binding protein HuR is essential for the B cell antibody response. *Nat. Immunol.* **16:** 415–425

Dobin A, Davis CA, Schlesinger F, Drenkow J, Zaleski C, Jha S, Batut P, Chaisson M & Gingeras TR (2013) STAR: ultrafast universal RNA-seq aligner. *Bioinformatics* **29:** 15–21

Dolezal E, Infantino S, Drepper F, Börsig T, Singh A, Wossning T, Fiala GJ, Minguet S, Warscheid B, Tarlinton DM, Jumaa H, Medgyesi D & Reth M (2017) The BTG2-PRMT1 module limits pre-B cell expansion by regulating the CDK4-Cyclin-D3 complex. *Nat. Immunol.* **18:** 911–920

Eden E, Navon R, Steinfeld I, Lipson D & Yakhini Z (2009) GOrilla: a tool for discovery and visualization of enriched GO terms in ranked gene lists. *BMC Bioinformatics* **10:** 48

Galloway A, Saveliev A, Łukasiak S, Hodson DJ, Bolland D, Balmanno K, Ahlfors H, Monzon-Casanova E, Mannurita SC, Bell LS, Andrews S, Diaz-Muñoz MD, Cook SJ, Corcoran A & Turner M (2016) RNA-binding proteins ZFP36L1 and ZFP36L2 promote cell quiescence. *Science* **352:** 453–459

Gerstberger S, Hafner M & Tuschl T (2014) A census of human RNA-binding proteins. *Nature Reviews Genetics 2013 14:7* **15:** 829–845

Giotti B, Chen S-H, Barnett MW, Regan T, Ly T, Wiemann S, Hume DA & Freeman TC (2018) Assembly of a Parts List of the Human Mitotic Cell Cycle Machinery. *J Mol Cell Biol* **32:** 2858

Györy I, Boller S, Nechanitzky R, Mandel E, Pott S, Liu E & Grosschedl R (2012) Transcription factor Ebf1 regulates differentiation stage-specific signaling, proliferation, and survival of B cells. *Genes Dev.* **26:** 668–682

Hardy RR & Hayakawa K (2003) B Cell Development Pathways. *https://doi.org/10.1146/annurev.immunol.19.1.595* **19:** 595–621

Hardy RR, Carmack CE, Shinton SA, Kemp JD & Hayakawa K (1991) Resolution and characterization of pro-B and pre-pro-B cell stages in normal mouse bone marrow. *Journal of Experimental Medicine* **173:** 1213–1225

Herzog S, Hug E, Meixlsperger S, Paik J-H, DePinho RA, Reth M & Jumaa H (2008) SLP-65 regulates immunoglobulin light chain gene recombination through the PI(3)K-PKB-Foxo pathway. *Nat. Immunol.* **9:** 623–631

Herzog S, Reth M & Jumaa H (2009) Regulation of B-cell proliferation and differentiation by pre-B-cell receptor signalling. *Nature Reviews Immunology* **9:** 195–205

Hobeika E, Thiemann S, Storch B, Jumaa H, Nielsen PJ, Pelanda R & Reth M (2006) Testing gene function early in the B cell lineage in mb1-cre mice. *PNAS* **103:** 13789–13794

Hu J, Qian H, Xue Y & Fu X-D (2018) PTB/nPTB: master regulators of neuronal fate in mammals. *Biophys Rep* **4:** 204–214

Inoue T, Morita M, Hijikata A, Fukuda-Yuzawa Y, Adachi S, Isono K, Ikawa T, Kawamoto H, Koseki H, Natsume T, Fukao T, Ohara O, Yamamoto T & Kurosaki T (2015) CNOT3 contributes to early B cell development by controlling Igh rearrangement and p53 mRNA stability. *Journal of Experimental Medicine* **212:** 1465–1479

Keene JD (2007) RNA regulons: coordination of post-transcriptional events. *Nature Reviews Genetics 2013 14:7* **8:** 533–543

Kim D, Ben Langmead & Salzberg SL (2015) HISAT: a fast spliced aligner with low memory requirements. *Nat. Methods* **12:** 357–360

Knoch K-P, Bergert H, Borgonovo B, Saeger H-D, Altkrüger A, Verkade P & Solimena M (2004) Polypyrimidine tract-binding protein promotes insulin secretory granule biogenesis. *Nature Cell Biology* **6:** 207–214

Knoch K-P, Nath-Sain S, Petzold A, Schneider H, Beck M, Wegbrod C, S nmez A, M nster C, Friedrich A, Roivainen M & Solimena M (2014) PTBP1 is required for glucose-stimulated cap-independent translation of insulin granule proteins and Coxsackieviruses in beta cells. *Molecular Metabolism* **3:** 518–530

König J, Zarnack K, Rot G, Curk T, Kayikci M, Zupan B, Turner DJ, Luscombe NM & Ule J (2010) iCLIP reveals the function of hnRNP particles in splicing at individual nucleotide resolution. *Nat. Struct. Mol. Biol.* **17:** 909–915

La Porta J, Matus-Nicodemos R, Valentín-Acevedo A & Covey LR (2016) The RNA-Binding Protein, Polypyrimidine Tract-Binding Protein 1 (PTBP1) Is a Key Regulator of CD4 T Cell Activation. *PLoS ONE* **11:** e0158708

Li Q, Zheng S, Han A, Lin C-H, Stoilov P, Fu X-D, Black DL & Blencowe BJ (2014) The splicing regulator PTBP2 controls a program of embryonic splicing required for neuronal maturation. *eLife Sciences* **3:** e01201

Li Z, Dordai DI, Lee J & Desiderio S (1996) A Conserved Degradation Signal Regulates RAG-2 Accumulation during Cell Division and Links V(D)J Recombination to the Cell Cycle. *Immunity* **5:** 575–589

Ling JP, Chhabra R, Merran JD, Schaughency PM, Wheelan SJ, Corden JL & Wong PC (2016) PTBP1 and PTBP2 Repress Nonconserved Cryptic Exons. *Cell Reports* **17:** 104–113

Llorian M, Schwartz S, Clark TA, Hollander D, Tan L-Y, Spellman R, Gordon A, Schweitzer AC, la Grange de P, Ast G & Smith CWJ (2010) Position-dependent alternative splicing activity revealed by global profiling of alternative splicing events regulated by PTB. *Nat. Struct. Mol. Biol.* **17:** 1114–1123

Love MI, Huber W & Anders S (2014) Moderated estimation of fold change and dispersion for RNA-seq data with DESeq2. **15:** 550

Lu R, Medina KL, Lancki DW & Singh H (2003) IRF-4,8 orchestrate the pre-B-to-B transition in lymphocyte development. *Genes Dev.* **17:** 1703–1708

Ma S, Pathak S, Mandal M, Trinh L, Clark MR & Lu R (2010) Ikaros and Aiolos Inhibit Pre-B-Cell Proliferation by Directly Suppressing c-Myc Expression. *Mol. Cell. Biol.* **30:** 4149–4158

Mandal M, Powers SE, Ochiai K, Georgopoulos K, Kee BL, Singh H & Clark MR (2009) Ras orchestrates exit from the cell cycle and light-chain recombination during early B cell development. *Nat. Immunol.* **10:** 1110–1117

Monzon-Casanova E, Screen M, Diaz-Muñoz MD, Coulson RMR, Bell SE, Lamers G, Solimena M, Smith CWJ & Turner M (2018) The RNA-binding protein PTBP1 is necessary for B cell selection in germinal centers. *Nat. Immunol.* **45:** 471

Nahar R, Ramezani-Rad P, Mossner M, Duy C, Cerchietti L, Geng H, Dovat S, Jumaa H, Ye BH, Melnick A & Müschen M (2011) Pre-B cell receptor–mediated activation of BCL6 induces pre-B cell quiescence through transcriptional repression of MYC. *Blood* **118:** 4174–4178

Nakamura N, Ramaswamy S, Vazquez F, Signoretti S, Loda M & Sellers WR (2000) Forkhead Transcription Factors Are Critical Effectors of Cell Death and Cell Cycle Arrest Downstream of PTEN. *Mol. Cell. Biol.* **20:** 8969–8982

Otto T & Sicinski P (2017) Cell cycle proteins as promising targets in cancer therapy. *Nature Reviews Cancer 2017 17:2* **17:** 93–115

Sadri N, Lu J-Y, Badura ML & Schneider RJ (2010) AUF1 is involved in splenic follicular B cell maintenance. *BMC Immunol* **11:** 1–14

Sasanuma H, Ozawa M & Yoshida N (2019) RNA-binding protein Ptbp1 is essential for BCR-mediated antibody production. *Int. Immunol.* **31:** 157–166

Schjerven H, McLaughlin J, Arenzana TL, Frietze S, Cheng D, Wadsworth SE, Lawson GW, Bensinger SJ, Farnham PJ, Witte ON & Smale ST (2013) Selective regulation of lymphopoiesis and leukemogenesis by individual zinc fingers of Ikaros. *Nat. Immunol.* **14:** 1073–1083

Schlissel M, Constantinescu A, Morrow T, Baxter M & Peng A (1993) Double-strand signal sequence breaks in V(D)J recombination are blunt, 5'-phosphorylated, RAG-dependent, and cell cycle regulated. *Genes Dev.* **7:** 2520–2532

Shen S, Park JW, Lu Z-X, Lin L, Henry MD, Wu YN, Zhou Q & Xing Y (2014) rMATS: robust and flexible detection of differential alternative splicing from replicate RNA-Seq data. *Proc. Natl. Acad. Sci. U.S.A.* **111:** E5593–601

Shibayama M, Ohno S, Osaka T, Sakamoto R, Tokunaga A, Nakatake Y, Sato M & Yoshida N (2009) Polypyrimidine tract-binding protein is essential for early mouse development and embryonic stem cell proliferation. *The FEBS Journal* **276:** 6658–6668

Shinkai Y, Rathbun G, Lam KP, Oltz EM, Stewart V, Mendelsohn M, Charron J, Datta M, Young F & Stall AM (1992) RAG-2-deficient mice lack mature lymphocytes owing to inability to initiate V(D)J rearrangement. *Cell* **68:** 855–867

Sibley CR, Blazquez L & Ule J (2016) Lessons from non-canonical splicing. *Nature Reviews Genetics 2013 14:7* **17:** 407–421

Spellman R, Llorian M & Smith CWJ (2007) Crossregulation and functional redundancy between the splicing regulator PTB and its paralogs nPTB and ROD1. *Molecular Cell* **27:** 420–434

Suckale J, Wendling O, Masjkur J, Jäger M, Münster C, Anastassiadis K, Stewart AF & Solimena M (2011) PTBP1 is required for embryonic development before gastrulation. *PLoS ONE* **6:** e16992

Sun X-H & Baltimore D (1991) An inhibitory domain of E12 transcription factor prevents DNA binding in E12 homodimers but not in E12 heterodimers. *Cell* **64:** 459–470

Susaki E, Nakayama K & Nakayama KI (2007) Cyclin D2 Translocates p27 out of the Nucleus and Promotes Its Degradation at the G0-G1 Transition. *Mol. Cell. Biol.* **27:** 4626–4640

Thompson BJ, Bhansali R, Diebold L, Cook DE, Stolzenburg L, Casagrande A-S, Besson T, Leblond B, Désiré L, Malinge S & Crispino JD (2015) DYRK1A controls the transition from proliferation to quiescence during lymphoid development by destabilizing Cyclin D3. *Journal of Experimental Medicine* **212:** 953–970

Trapnell C, Roberts A, Goff L, Pertea G, Kim D, Kelley DR, Pimentel H, Salzberg SL, Rinn JL & Pachter L (2012) Differential gene and transcript expression analysis of RNA-seq experiments with TopHat and Cufflinks. *Nat Protoc* **7:** 562–578

Urbánek P, Wang ZQ, Fetka I, Wagner EF & Busslinger M (1994) Complete block of early B cell differentiation and altered patterning of the posterior midbrain in mice lacking Pax5/BSAP. *Cell* **79:** 901–912

Vervoorts J & Lüscher B (2008) Post-translational regulation of the tumor suppressor p27<Superscript>KIP1</Superscript>. *Cell. Mol. Life Sci.* **65:** 3255–3264

Vilagos B, Hoffmann M, Souabni A, Sun Q, Werner B, Medvedovic J, Bilic I, Minnich M, Axelsson E, Jaritz M & Busslinger M (2012) Essential role of EBF1 in the generation and function of distinct mature B cell types. *J. Exp. Med.* **209:** 775–792

Vuong JK, Lin C-H, Zhang M, Chen L, Black DL & Zheng S (2016) PTBP1 and PTBP2 Serve Both Specific and Redundant Functions in Neuronal Pre-mRNA Splicing. *Cell Reports* **17:** 2766–2775

Yamazaki T, Liu L & Manley JL (2019) TCF3 Mutually Exclusive Alternative Splicing Is Controlled by Long Range Cooperative Actions between hnRNPH1 and PTBP1. *RNA* **25:** rna.072298.119–1508

Yang C-Y, Ramamoorthy S, Boller S, Rosenbaum M, Rodriguez Gil A, Mittler G, Imai Y, Kuba K & Grosschedl R (2016) Interaction of CCR4–NOT with EBF1 regulates gene-specific transcription and mRNA stability in B lymphopoiesis. *Genes Dev.* **30:** 2310–2324

Yang W, Shen J, Wu M, Arsura M, FitzGerald M, Suldan Z, Kim DW, Hofmann CS, Pianetti S, Romieu-Mourez R, Freedman LP & Sonenshein GE (2001) Repression of transcription of the p27 Kip1 cyclin-dependent kinase inhibitor gene by c-Myc. *Oncogene* **20:** 1688–1702

Yoon M-K, Mitrea DM, Ou L & Kriwacki RW (2012) Cell cycle regulation by the intrinsically disordered proteins p21 and p27. *Biochemical Society Transactions* **40:** 981–988

Yüce Ö, Piekny A & Glotzer M (2005) An ECT2–centralspindlin complex regulates the localization and function of RhoA. *The Journal of Cell Biology* **170:** 571–582

Zhu A, Ibrahim JG & Love MI (2019) Heavy-tailed prior distributions for sequence count data: removing the noise and preserving large differences. *Bioinformatics* **35:** 2084–2092

Legends

Figure 1. Absence of PTBP1 and PTBP2 blocks B cell development.

(A), Numbers of B cells ($B220^{+}CD19^{+}$) in spleens of mice with the indicated genotypes. Data points are from individual mice. Arithmetic means are shown with lines.

(B) Flow cytometry of splenocytes to identify B cells. Numbers shown are proportions of gated B cells. Events shown were pre-gated on live ($eFluor780^{-}$) single cells.

(C) Gating strategy based on cell-surface markers for developing B cells from bone marrow cells pre-gated on dump (Gr-1, CD11b, NK1.1, Siglec-F and F4/80)-negative live ($eFluor780^{-}$) cells.

(D) Number of developing B cells in the bone marrow (2 femurs and 2 tibias per mouse) of mice with the indicated genotypes. Data shown are from one representative out of three independent experiments carried out with the same mouse genotypes shown except for $CD79a^{Cre/+}Ptbp1^{+/+}Ptbp2^{+/+}$ mice which were only included in the experiment shown here. Bars depict means, each point represents data from an individual mouse and P-values were calculated by one-way ANOVA with Tukey's multiple comparisons test. Summary adjusted p value *<0.05, **<0.01, ***<0.001, ****<0.0001.

Figure 2. PTBP1 and PTBP2 absence causes changes in mRNA abundance and AS.

(A) Differences in mRNA abundance in pairwise comparisons from pro-B cell transcriptomes. Shown are Log2Fold changes calculated with DESeq2 (Table S3). Red dots are values from genes with significant differences in mRNA abundance (padj value <0.05) with a |Log2Fold change| > 0.5. Grey dots are values from genes with no significant differences (padj >0.05) or with a |Log2Fold change| < 0.5. Numbers in plots are the number of genes with increased or decreased mRNA abundance.

(B) Differences in AS in pairwise comparisons from pro-B cells. Shown are |inclusion level differences| >0.1 with an FDR<0.05 for different types of alternatively spliced events (Figure S4C): skipped exons (SE), mutually exclusive exons (MXE), alternative 5' and 3' splice sites (A5SS and A3SS, respectively), and retained introns (RI), (Table S4) analysed with rMATS. Each dot shows the inclusion level difference for one event.

(C) Overlaps of genes that have changes in abundance and AS.

(D) Heatmap shows z-scores of normalised read counts from DESeq2 from each biological replicate for genes that were found with differential mRNA abundance in any of the three pair-wise comparisons shown in A.

(E) Heatmap shows z-scores of inclusion levels from each biological replicate for those AS events that are alternatively spliced in any of the three pairwise comparisons shown in B.

(D, E) Unsupervised hierarchical clustering was done on Euclidean distances from z-scores and is shown with dendrograms.

Figure 3. PTBP1 regulates pathways associated with growth and proliferation

(A) *Ebf1*, *Foxo1* and *IL7r* mRNA abundance in pro-B cells from control, P1sKO and P1P2dKO mice.

(B) PTBP1 binding (iCLIP data) to the *Foxo1* 3'UTR.

(C) IL-7R (CD127) geometric mean fluorescent intensity in stages of B cell development identified as shown in Figure 1C. Individual data points are from individual mice. Data shown is from one representative out of two experiments. Unpaired T-test was carried out comparing control and P1P2dKO developing B cells. p values were > 0.05 and are not shown.

(D) Selected gene ontology (GO) terms (process and function) significantly (p-value <0.05) enriched amongst genes that are differentially expressed at the abundance or the AS level when comparing the transcriptome of P1P2dKO pro-B cells to P1sKO and control pro-B cells as shown in Figure 2D and 2E. Numbers show how many genes a GO term relates to. Table S5 contains all significantly enriched GO process and function terms.

(E) mRNA abundance of CDK inhibitors in pro-B cells from control, P1sKO and P1P2dKO mice.

(A and E) Points show DESeq2 normalised read counts from individual pro-B cell mRNAseq libraries. Bars depict arithmetic means. DESeq2 calculated p-adjusted values are shown when <0.05 for the indicated pairwise comparisons.

Figure 4. Enhanced entry into S-phase and block at G2 in P1P2dKO pro-B cells.

(A) EdU and BrdU sequential labelling experimental set up to distinguish early, late and post S-phase cells.

(B) Flow cytometry data of the different stages of S-phase in pro-B cells ($B220^{+}CD19^{+}IgD^{-}$ $surfaceIgM^{-}intracellular\text{-}Ig\mu^{-}CD43^{high}$) identified as shown in Figure S5D**.** Numbers shown are proportions of cells.

(C) Percentages of pro-B cells in different S-phase stages determined as shown in A and B.

(D) Flow cytometry data of pro-B cells identified as shown in Figure S5D and excluding $BrdU^{+}$-only (cells in early S-phase). Numbers shown are proportions of cells in the G2/M gate.

(E) Proportions and numbers (in 2 femurs and 2 tibias per mouse) of pro-B cells in G2/M identified as shown in (D).

(F) Phospho-histone 3 serine 10 (pH3 S10) staining amongst FrB pro-B cells identified as in Figure S5A.

(G) Percentages of pH3(S10)-positive cells amongst cells with 4N DNA amounts in pro-B cells (FrB) assessed by flow cytometry as shown in F.

(C, E, G) Bars depict arithmetic means, each point represents data from an individual mouse and P-values were calculated by one-way ANOVA with Tukey's multiple comparisons test. Summary adjusted p-value *<0.05, **<0.01, ***<0.001, ****<0.0001. (B-E) Data shown are from one of two independent experiments. (F, G) Data shown are from one out of three independent experiments.

Figure 5. PTBP1 controls CDK activity in pro-B cells.

(A) Intracellular flow cytometry with anti-p27 antibody or control isotype staining detected with an anti-rabbit AF647-conjugated secondary antibody.

(B) Median fluorescence intensities (MFI) from staining shown in A.

(C) Intracellular flow cytometry with the indicated antibodies. Numbers show proportions of gated events.

(D) Proportions of cells identified in C.

(A, C) Each histogram line shows data from an individual mouse with the indicated genotype. FrB pro-B cells in G0/G1, S or G2/M phases of the cell cycle were defined by EdU incorporation and DNA staining as shown in Figure S5A.

(B, C) Points show data from individual mice. Bars depict arithmetic means. P-values were calculated by two-way ANOVA with Tukey's multiple comparisons test. Summary adjusted p value *<0.05, **<0.01, ***<0.001, ****<0.0001.

(A-D) Data are from one experiment with four to five mice per genotype. The differences observed for pT592-SAMHD1 and pS807/S811-RB between control and P1P2dKO cells

were confirmed in an independent experiment where two control and two P1P2dKO mice were used.

Figure 6. PTBP1 controls expression of genes important for S-phase entry.

(A) Log2-fold changes in mRNA abundance in the indicated pairwise comparisons for all tested genes (all genes), genes with increased abundance in S-phase (S) and G2/M-phases (G2/M). Grey dots show genes with padj>0.05. Red dots amongst "all genes" show genes with padj<0.05 and a |log2-fold change| >0.5. Red dots amongst S and G2M groups show genes with a padj<0.05 regardless of their log2-fold change.

(B) mRNA abundance in pro-B cells from control, P1sKO and P1P2dKO mice. *Rbl1* (name in yellow) is predicted to have reduced mRNA abundance due to changes in AS triggering NMD upon *Ptbp1* and *Ptbp2* deletion. Individual data points show DESeq2 normalised read counts from individual pro-B cell mRNAseq libraries. Bars depict arithmetic means. DESeq2 calculated adjusted p-values are shown when <0.05 for the indicated pairwise comparisons.

(C) Intracellular c-MYC or control isotype staining of FrB pro-B cells in different stages of the cell cycle identified as shown in Figure S5A.

(D) Median fluorescence intensities (MFI) from the staining shown in (C). Each point shows data from an individual mouse. Bars show means. P-values were calculated by two-way ANOVA with Tukey's multiple comparisons test. Summary adjusted p value *<0.05, **<0.01, ***<0.001, ****<0.0001. Data shown are from one representative out of two independent experiments.

(E) PTBP1 iCLIP and mRNAseq data visualisation. For PTBP1 iCLIP, x-link sites are shown for all events. Clusters of PTBP1 binding are shown when found. mRNAseq data from pro-B cells of one replicate per genotype is shown using sashimi plot visualisation from

Integrative Genomics Viewer (IGV). Numbers on the left show the maximum number of reads in the coverage plots. Arcs depict exon-exon junctions detected in mRNAseq reads. Numbers in arcs show the number of reads for the depicted exon-exon junction. Parts of transcript isoforms predicted to be degraded by NMD are shown in yellow. Parts of transcript isoforms coding for proteins are shown in blue. Exon numbers of transcript isoforms coding for proteins are shown with E and a number.

(F) mRNAseq visualisation as in (E) from HeLa control cells or cells where PTBP1 and PTBP2 were knocked down (Ling *et al*, 2016).

(G) Human *RBL1* normalised DESeq2 read counts from the two mRNAseq libraries (one control and 1 double knock down) shown in (F).

Figure 7. PTBP1 controls expression of genes important for mitosis.

(A) mRNA abundance of the indicated genes. Genes whose names are in yellow and bold are predicted to have reduced mRNA abundance due to changes in AS triggering NMD upon *Ptbp1* and *Ptbp2* deletion. Individual data points show DESeq2 normalised read counts from individual pro-B cell mRNAseq libraries. Bars depict arithmetic means. DESeq2 calculated adjusted p-values are shown when <0.05 for the indicated pairwise comparisons.

(B) PTBP1 iCLIP and mRNA-Seq visualisation as described in Figure 6E.

(C) Representation of cell cycle mRNA regulon controlled by PTBP1 in pro-B cells and consequences of *Ptbp1* and *Ptbp2* deletion in pro-B cells. Depicted interactions of PTBP1 with individual factors are likely to be direct.

Supplementary Figures:

Figure S1. Expression of PTBP in B cell development.

(A) Representation of B cell development in the bone marrow using the Philadelphia nomenclature (Hardy & Hayakawa, 2003) including Hardy's fractions (Fr) based on cell-surface markers (Hardy *et al*, 1991).

(B) Identification strategy for bone marrow cells using cell-surface and intracellular markers.

(C) Expression of PTBP1, PTBP2 and PTBP3 analysed by flow cytometry. Identification of different B cell developmental stages was carried out as shown in B.

(D) Geometric mean fluorescence intensity (gMFI) of staining for anti-PTBP1, PTBP2, PTBP3 and isotype control antibodies as shown in C. Bars depict arithmetic means. Each data point shows data from an individual control mouse (*CD79a*$^{+/+}$*Ptbp1*$^{fl/fl}$*Ptbp2*$^{fl/fl}$). Data shown are from one experiment with 5 mice.

(E) Numbers and proportions of B cells (B220^{+}CD19^{+}) in mesenteric lymph nodes.

Figure S2. B cell development in the absence of PTBP1 and PTBP2.

(A) c-KIT and CD2 staining at different B cell developmental stages gated as shown in Figure 1C in mice of the indicated genotypes.

(B) c-KIT median fluorescence intensity (MFI) in pro-B cells (FrB and FrC) identified as shown in A. Data shown is from one out of three independent experiments.

(C) Cell surface and intracellular staining strategy to define B cell developmental stages using Igμ staining in bone marrow cells from mice of the indicated genotypes. Numbers shown are percentages of gated events.

(D) Numbers of developing B cells in bone marrow from two femurs and two tibias identified as shown in C. Data shown are from one experiment.

(E) PTBP1, PTBP2 and PTBP3 detection and negative isotype control staining in different B cell developmental stages identified as shown in C. Data shown are of a representative mouse out of five for each indicated genotype. Data shown are from one experiment.

(B, E) Bars show arithmetic means, each point represents data from an individual mouse and P-values were calculated by one-way ANOVA with Tukey's multiple comparisons test. Summary adjusted p value *<0.05, **<0.01, ***<0.001, ****<0.0001.

Figure S3. Cell sorting strategy of pro-B cells.

Cell sorting strategy of FrB pro-B ($B220^{+}CD19^{+}IgM^{-}IgD^{-}CD2^{-}CD43^{high}CD25^{-}cKIT^{+}CD24^{+}CD249^{+}$) cells used to isolate RNA and carry out mRNAseq libraries. “Dump” contains excluded cells stained with anti-IgM, anti-CD2 and streptavidin. Prior sorting, bone marrow cells were depleted from Gr-1, CD11b, IgD, NK1.1, CD3e and Ter119-positive cells using biotinylated antibodies.

Figure S4. Transcriptome analysis of pro-B cells.

(A) Transcriptome correlation in mitogen-activated primary B cells and FrB pro-B cells. Dots show mean values of TPMs (transcripts per million) from four or five biological replicates in mitogen-activated B cells and pro-B cells, respectively. Correlation was calculated with Spearman's rank correlation rho on genes with >= 1 TPM in pro-B cells and >0 TPM in mitogen-activated B cells (12545 genes). 681 genes had 0 TPMs in mitogen-activated B cells and >=1 TPM in pro-B cells.

(B) Proportions of genes with differences in mRNA abundance for the indicated pairwise comparisons that are bound by clusters of PTBP1 (iCLIP data) on their 3’UTR (Tables S2 and S3).

(C) Different types of alternative splicing events analysed with rMATS.

(D) Proportions of AS changes between the indicated comparisons that are bound by at least one PTBP1 cluster on the alternatively spliced exon or in its vicinity (500 nucleotides upstream or downstream of the alternatively spliced exon, on the constitutive flanking exons, on the 500 nucleotides downstream of the upstream constitutive exon or on the 500 nucleotides upstream of the downstream constitutive exon) (Tables S2 and S4).

(E) mRNA abundance of known regulators of B cell development in pro-B cells. DESeq2 normalised read counts of the indicated genes. DESeq2 calculated padj values are shown when <0.05. Bars show arithmetic means. Each dot shows data from an individual mRNAseq biological replicate.

Figure S5. Cell cycle analysis in developing B cells.

(A) Identification strategy for proliferating FrB pro-B cells amongst bone marrow cells from mice with the indicated genotypes. Mice were injected with EdU i.p. one hour before analysis to track cells in G0/G1, S and G2/M phases of the cell cycle.

(B) Proportions of FrB developing B cells in G0/G1, S and G2/M phases defined as in A. Data shown are from one out of three independent experiments.

(C) FCS-A measurements of FrB pro-B cells in different phases of the cell cycle identified as in A.

(D) Gating strategy to identify pre-pro-, pro- and early-pre-B cells in EdU and BrdU sequential labelling experiments (Figure 4A) in live bone marrow cells from the indicated genotypes.

(E) Early-, late- and post-S-phase gating amongst pre-pro-, pro- and early-pre-B cells identified as shown in D.

(F) Proportions of early, late and post S-phase cells amongst pre-pro-, pro- and early-pre-B cells identified as shown in D and E. Data shown are from one out of two independent experiments.

(B, C and F) Bars show arithmetic means, each point shows data from an individual mouse and P-values were calculated by one-way ANOVA with Tukey's multiple comparisons test. Summary adjusted p-value *<0.05, **<0.01, ***<0.001, ****<0.0001.

Figure S6. PTBP1 binding to target transcripts.

PTBP1 binding (iCLIP data) to 3'UTRs.

SUPPLEMENTAL TABLES:

Table S1. PTBP1 binding sites (xlinks).

Table S2. PTBP1 binding sites (clusters).

Table S3. mRNA abundance analysis. DESeq2 results shown in Figure 2A. Separate tabs show genes with significant differential (padj<0.05) mRNA abundance with a |log2 fold change| > 0.5 for the different pairwise comparisons carried out and also all the results obtained with DESeq2. Additional tabs show genes whose transcripts were bound by PTBP1 clusters at their 3'UTR.

Table S4. AS analysis. Different tabs show inclusion level differences (IncLevelDifference) shown in Figure 2B for the three pairwise comparisons carried out. The first three tabs show significant (FDR <0.05) alternative splicing events with an absolute inclusion level difference >0.1. "allresults" tabs show all the results from rMATS. "PTBP1 bound" tabs show those significantly differential splicing events that were bound in their vicinity by PTBP1 clusters.

Table S5. Gene ontology enrichment analysis. Results from gene ontology enrichment analysis carried out with the groups of genes identified in Figure 2D and Figure 2E.

Table S6. DESeq2 results for genes shown to have high mRNA expression levels in S or G2M phases (Giotti *et al,* 2018) in the three pair-wise comparisons shown in Figure 6A.

Table S7. Antibodies and reagents used in flow cytometry experiments.

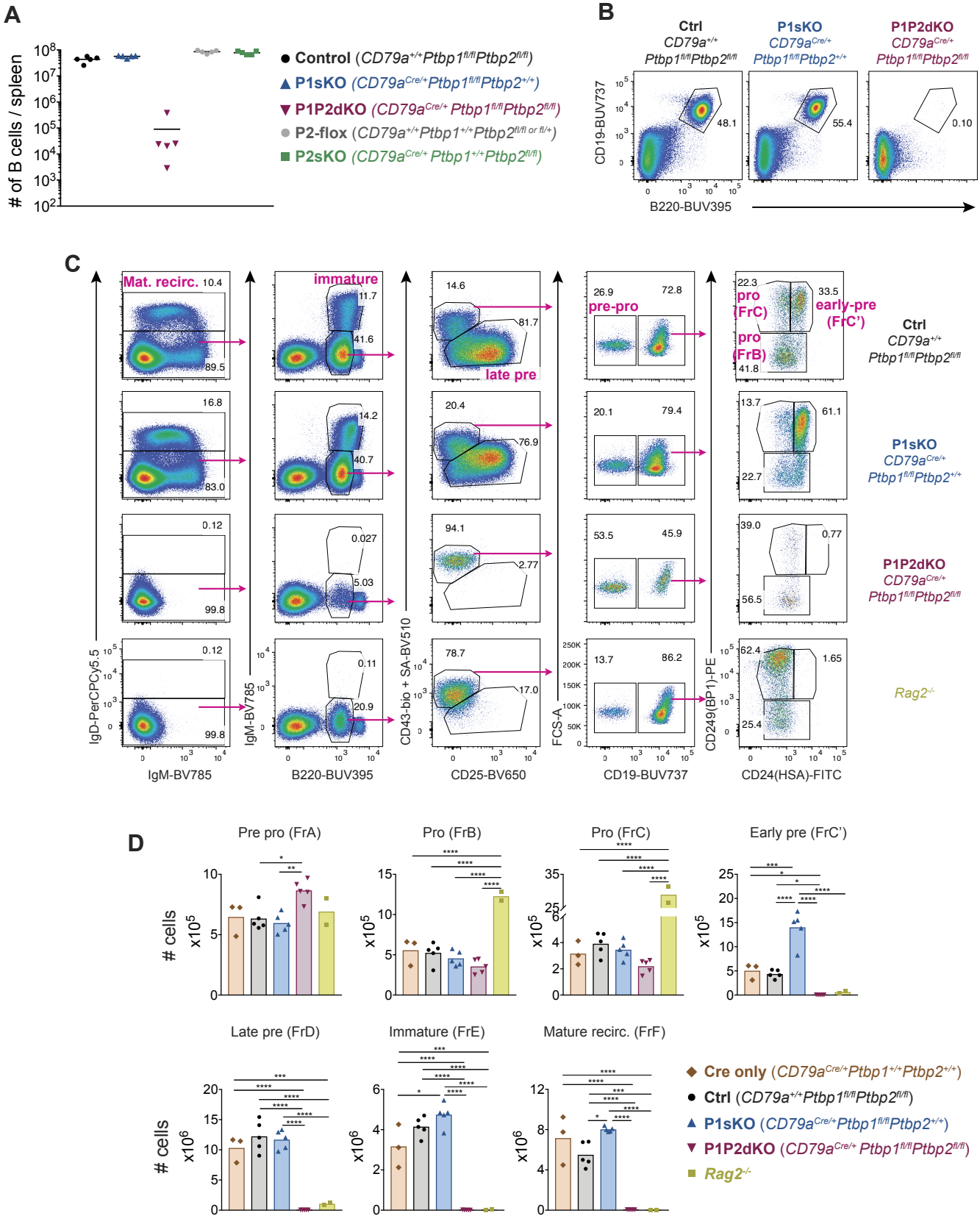

Figure 1

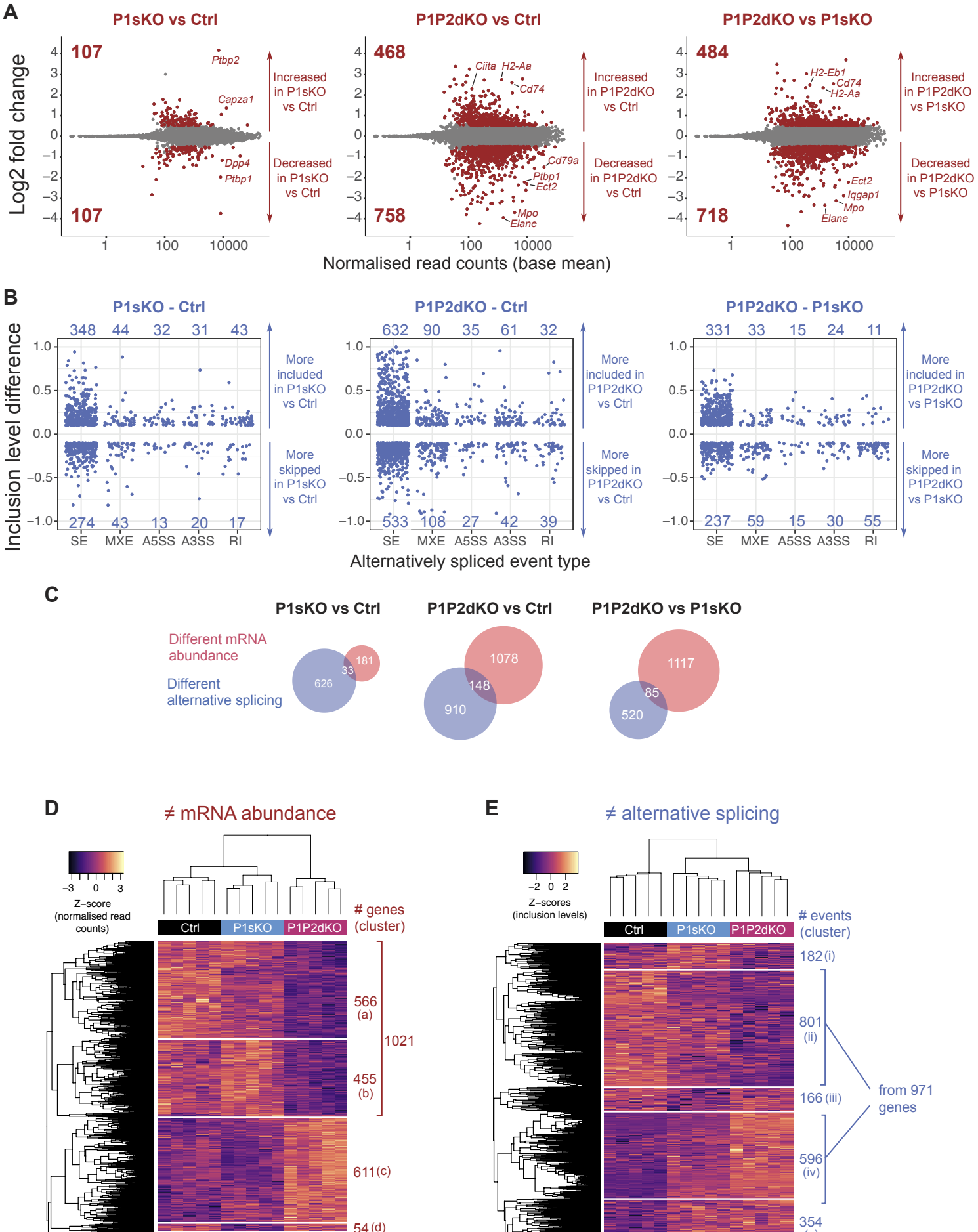

Figure 2

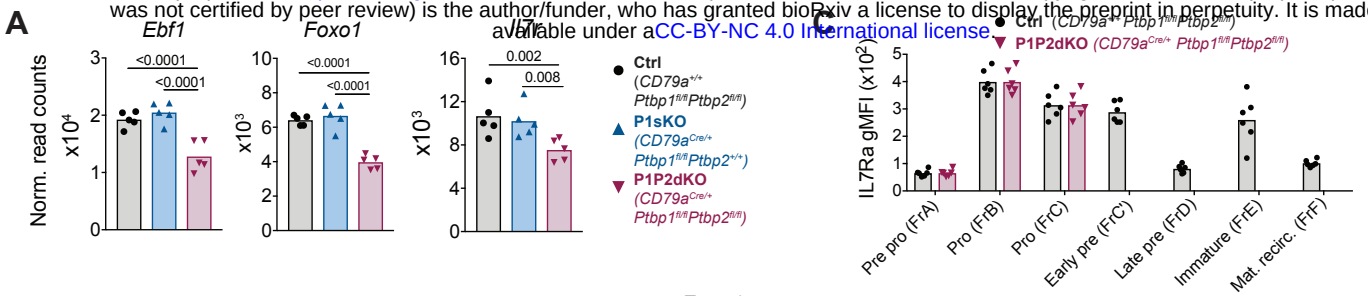

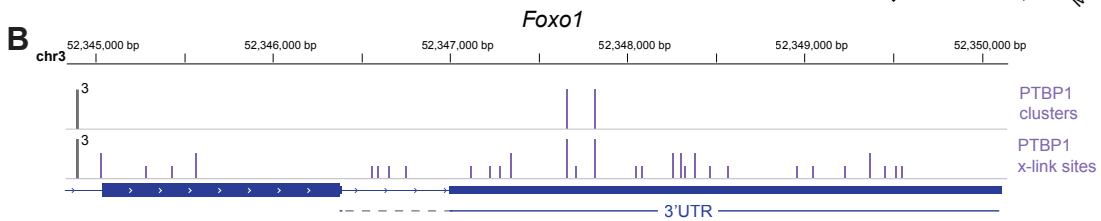

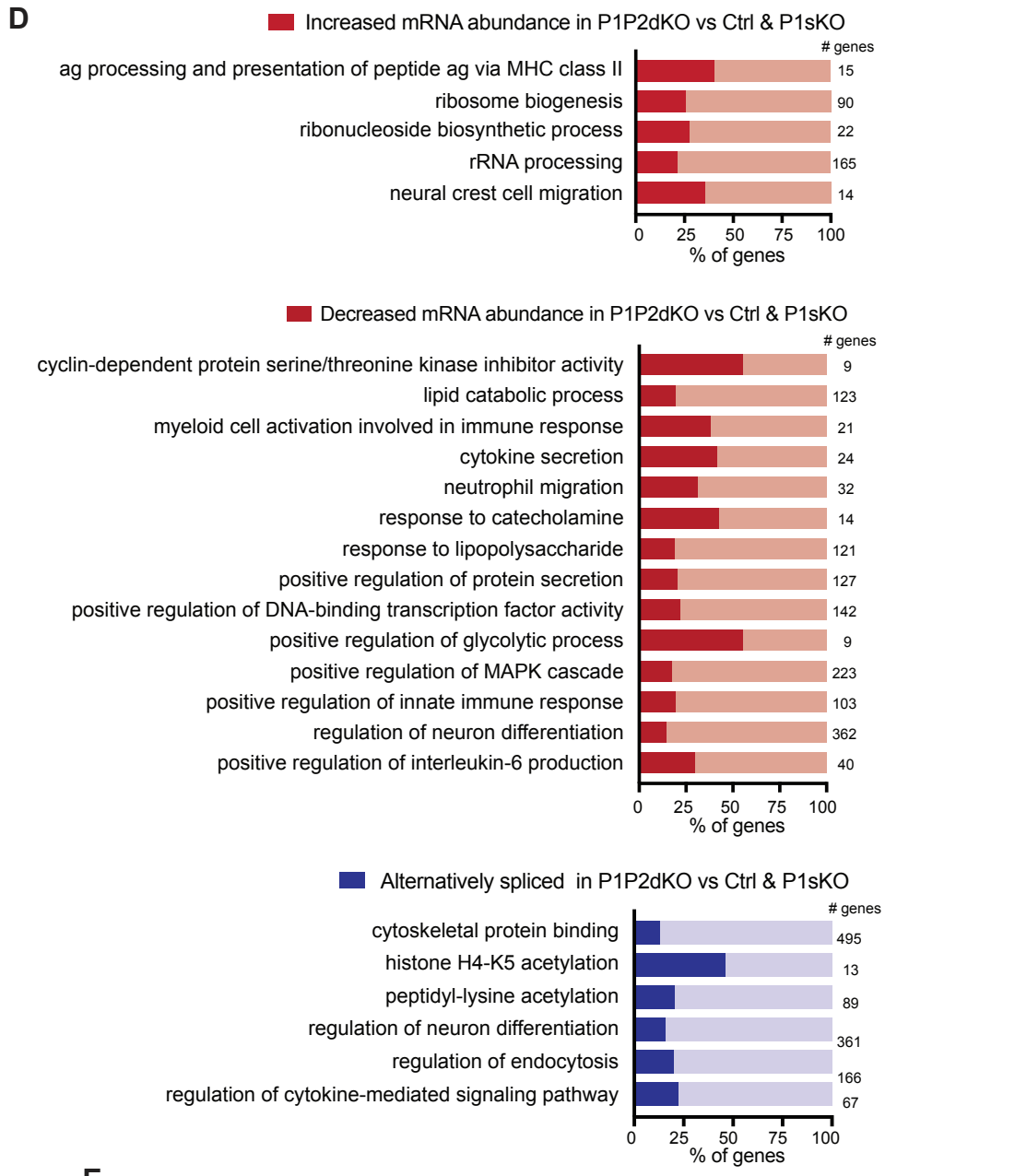

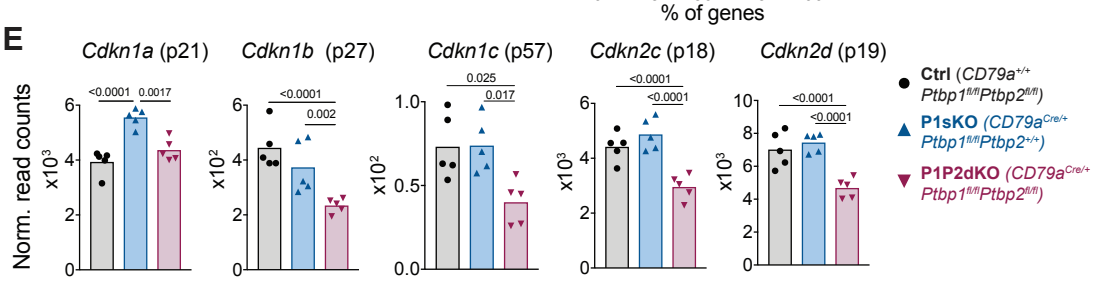

Figure 3

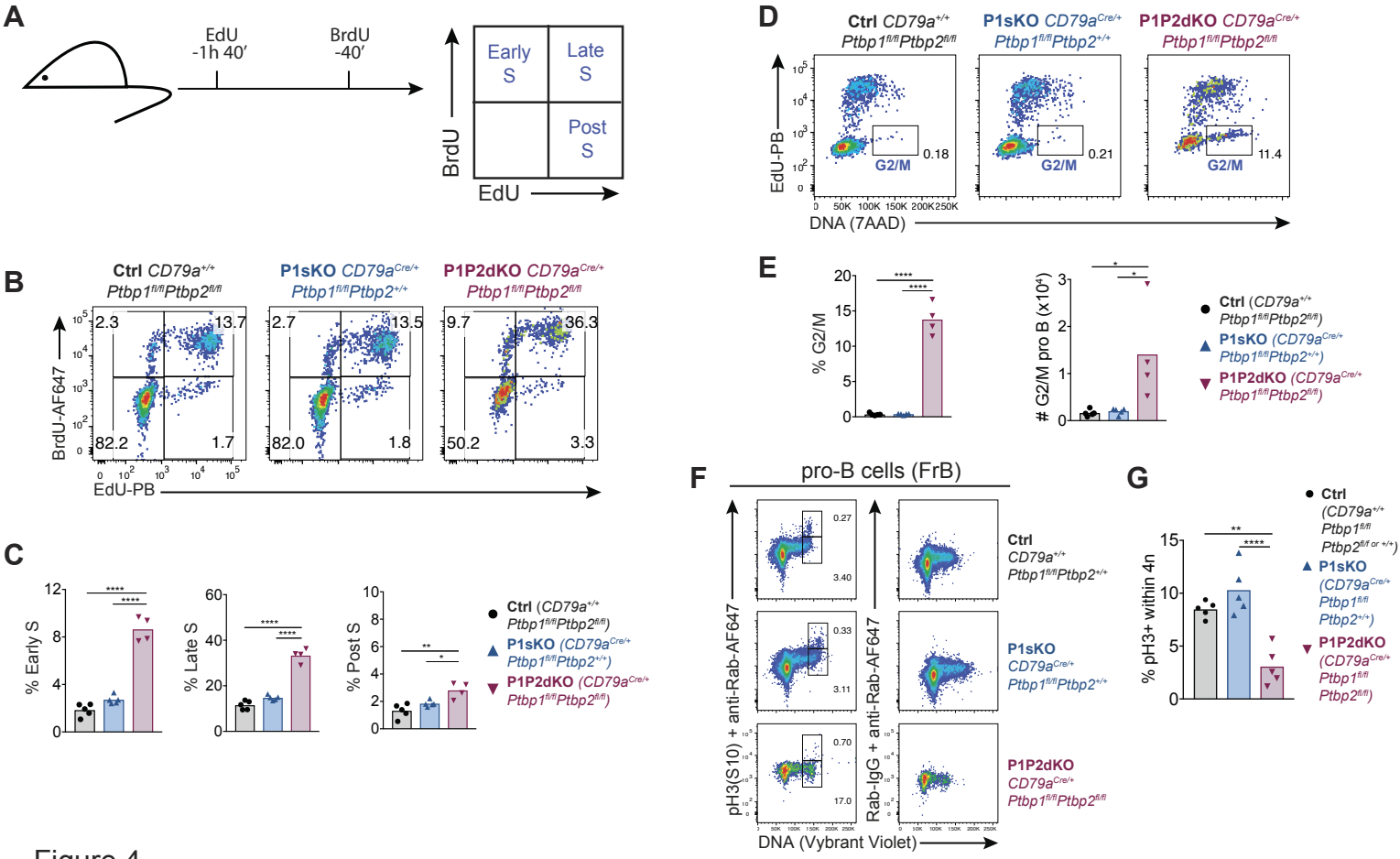

Figure 4

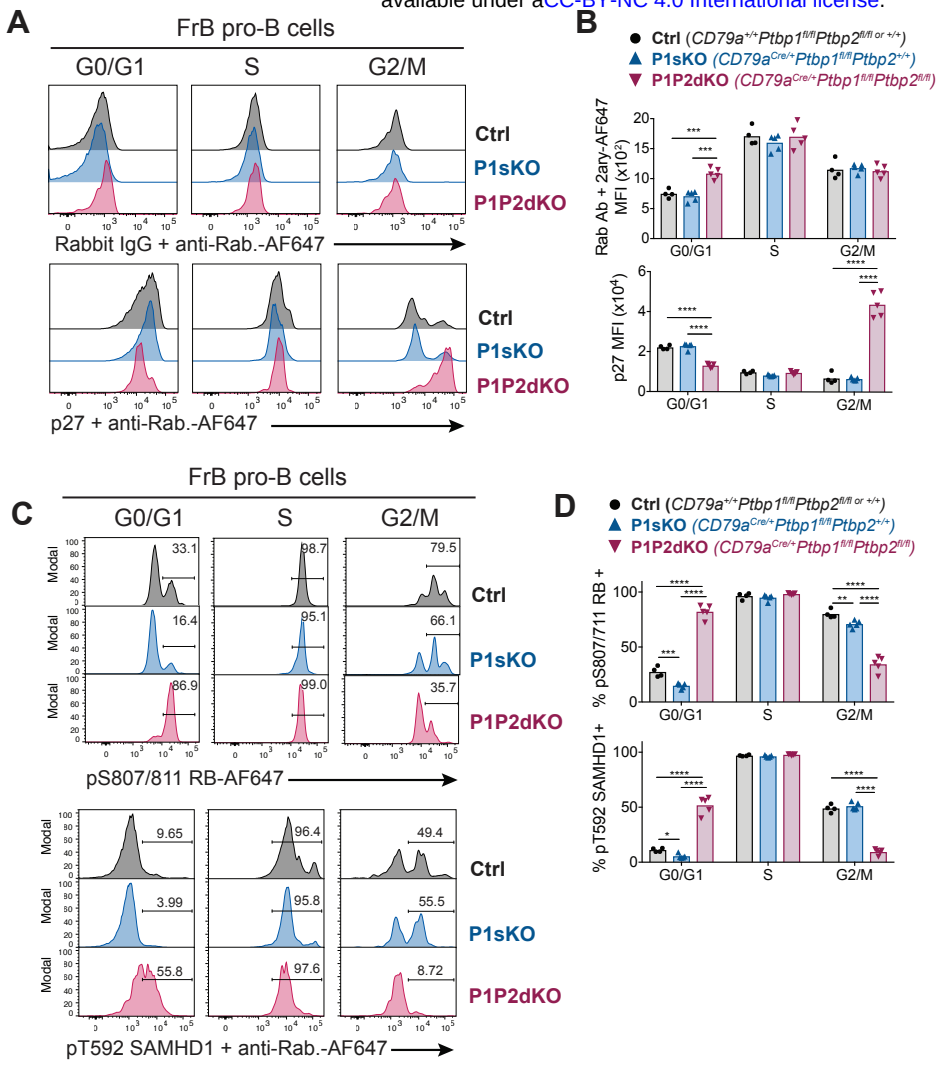

Figure 5

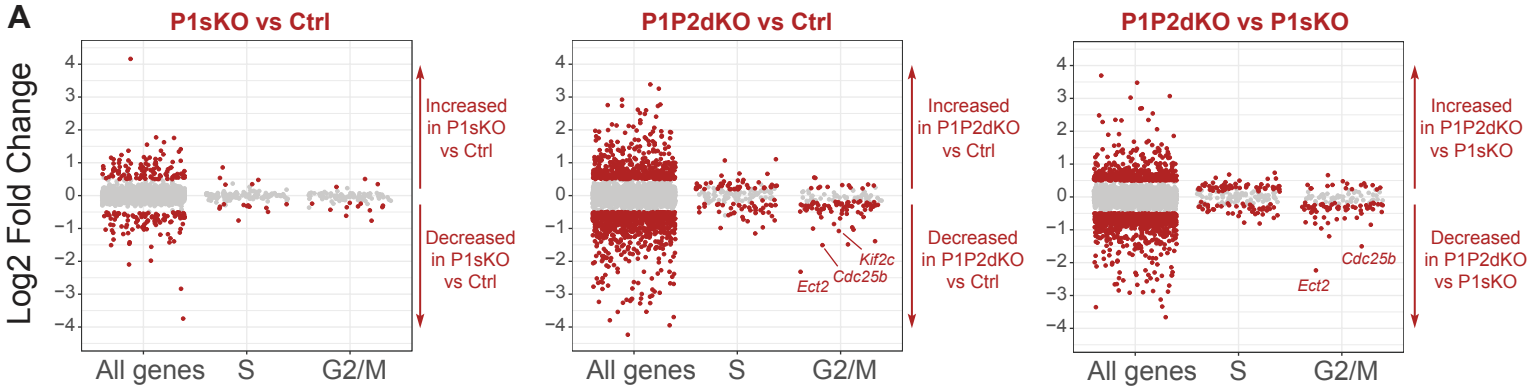

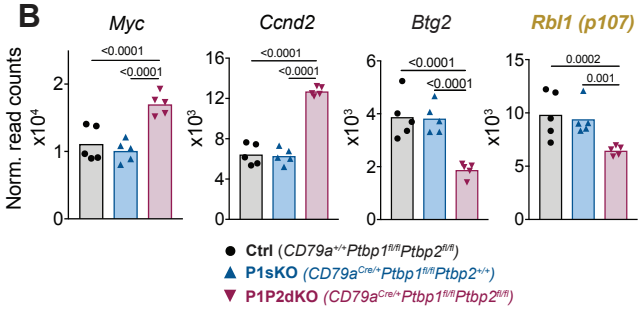

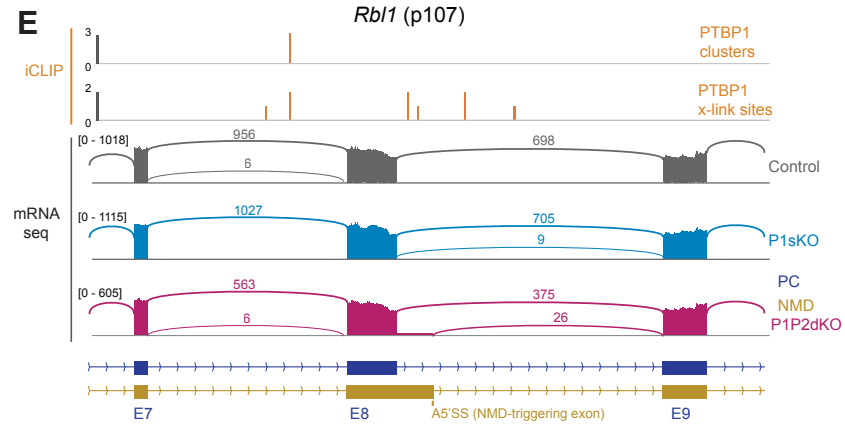

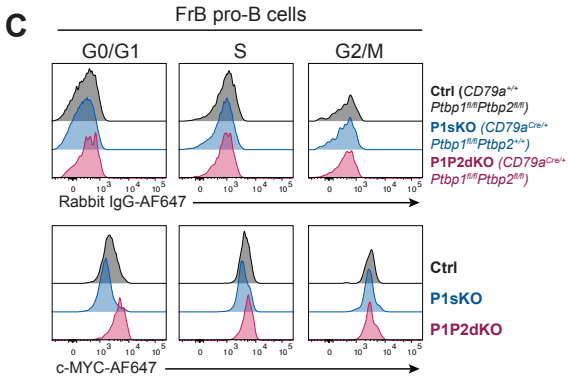

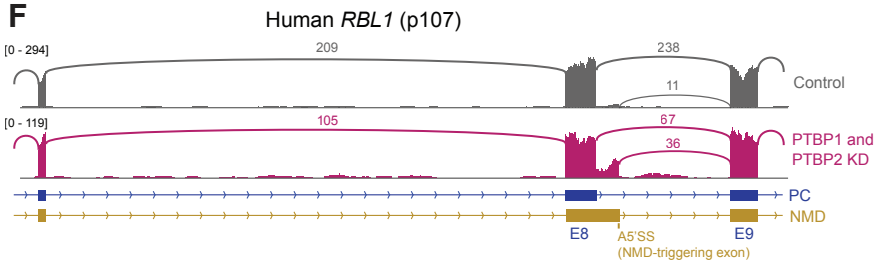

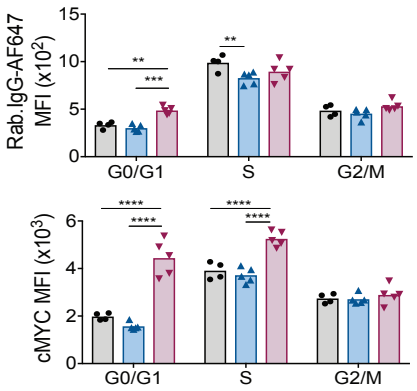

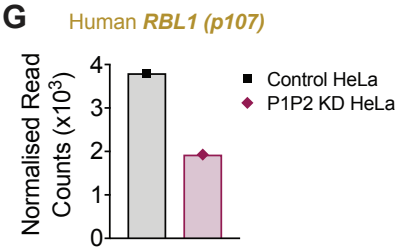

Figure 6

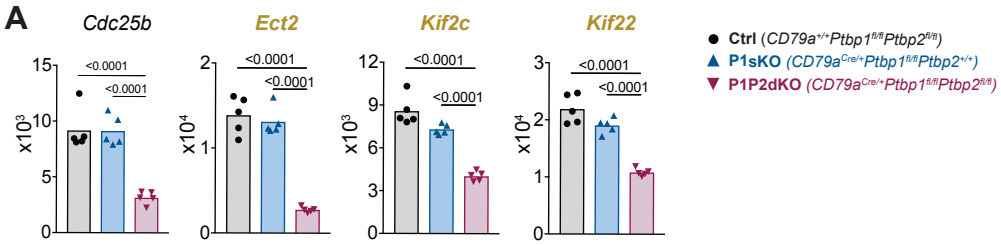

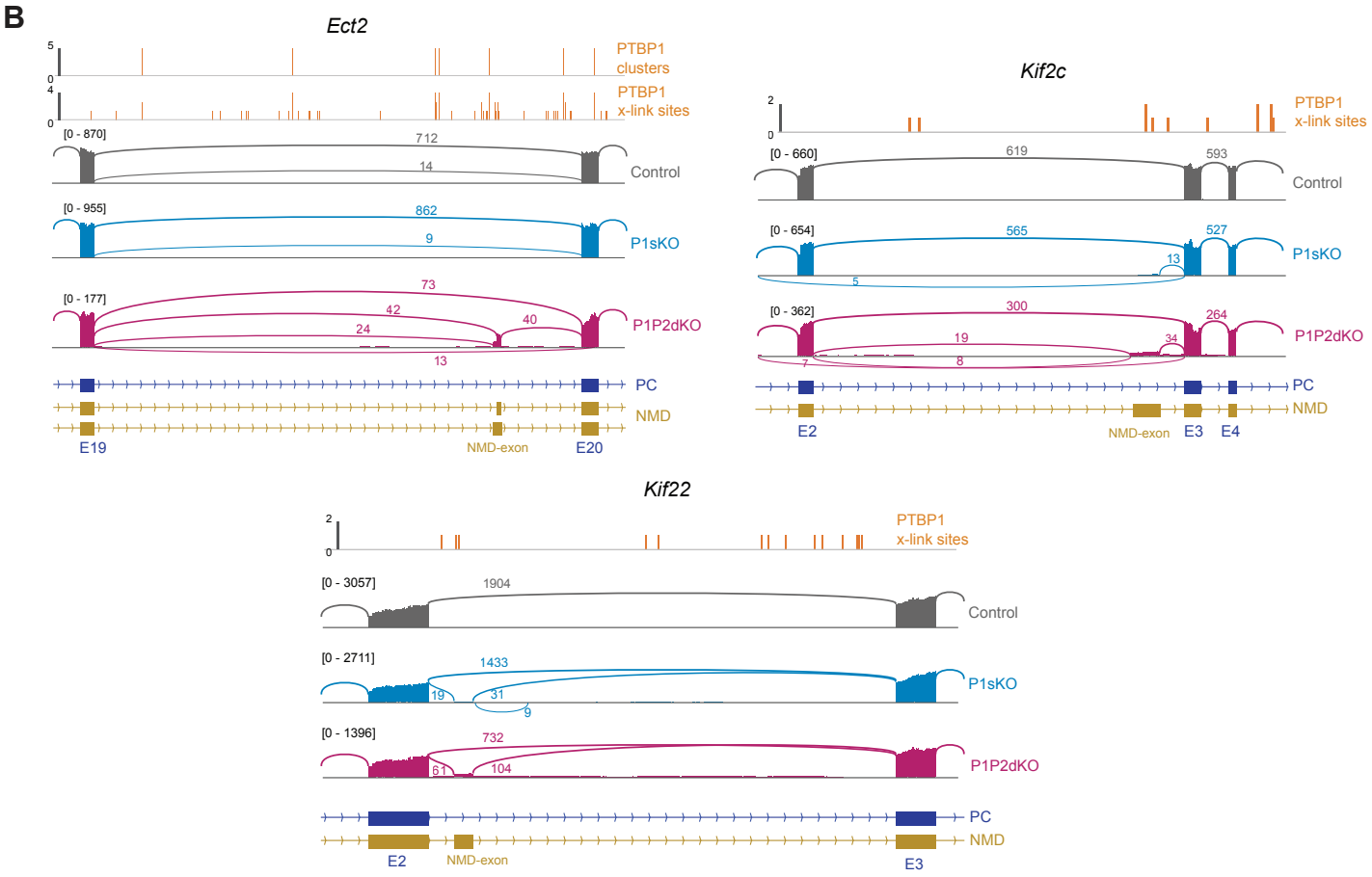

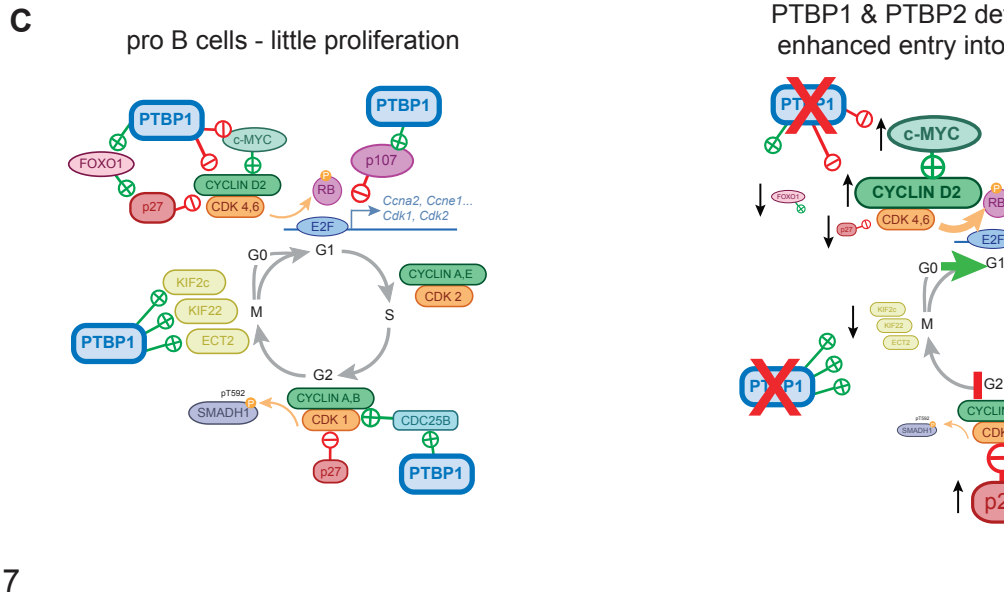

Figure 7